

Journal of Materials Chemistry A

Materials for energy and sustainability

Accepted Manuscript

This article can be cited before page numbers have been issued, to do this please use: P. Basyach, A. K. Guha, S. Borthakur, L. Kalita, P. Chetia, K. Sonowal and L. Saikia, *J. Mater. Chem. A*, 2020, DOI: 10.1039/D0TA03729J.



This is an Accepted Manuscript, which has been through the Royal Society of Chemistry peer review process and has been accepted for publication.

Accepted Manuscripts are published online shortly after acceptance, before technical editing, formatting and proof reading. Using this free service, authors can make their results available to the community, in citable form, before we publish the edited article. We will replace this Accepted Manuscript with the edited and formatted Advance Article as soon as it is available.

You can find more information about Accepted Manuscripts in the [Information for Authors](#).

Please note that technical editing may introduce minor changes to the text and/or graphics, which may alter content. The journal's standard [Terms & Conditions](#) and the [Ethical guidelines](#) still apply. In no event shall the Royal Society of Chemistry be held responsible for any errors or omissions in this Accepted Manuscript or any consequences arising from the use of any information it contains.

Efficient hydroxylation of benzene to phenol by H₂O₂ using Ni doped CuWO₄ on carbon nitride as catalyst under solar irradiation and its structure activity correlation

View Article Online
DOI: 10.1039/D0TA03729J

Purashri Basyach,^{a,b} Ankur Kanti Guha,^c Sukanya Borthakur,^{a,b} Lisamoni Kalita,^{a,b} Pubali Chetia,^{a,b} Karanika Sonowal^{a,b} and Lakshi Saikia^{*a,b}

^a Advanced Materials Group, Materials Sciences & Technology Division, CSIR-North East Institute of Science and Technology, Jorhat-785006, Assam, India

^b Academy of Scientific and Innovative Research, New Delhi, India

^c Department of Chemistry, Cotton University, Panbazar, Guwahati-781001

Abstract: A series of environmentally benign and highly efficient Z-scheme Ni doped CuWO₄ on graphitic carbon nitride (g-C₃N₄) were synthesized. The Ni-CuWO₄ nanoparticles were prepared through substitution of Ni²⁺ on wolframite CuWO₄ crystal. The photocatalytic activity of these nanocomposites was investigated for the hydroxylation of benzene to phenol considering the importance of phenol and carcinogenicity of benzene. Excellent benzene conversion of 98.5% with 82.7% selectivity and 81.5% yield of phenol was achieved over 0.2% Ni-CuWO₄/g-C₃N₄ in 15 minutes under sunlight using H₂O₂ as oxidant in water which is higher than those of pristine g-C₃N₄ and Ni-CuWO₄. The high yield of phenol was mainly attributed to the narrow band gap of the semiconductor and enhanced visible light absorption capacity over a specific range of wavelength by the introduction of g-C₃N₄ which minimized the rapid recombination of photogenerated holes and electrons. The computational study related to this work also implied the high optical property and stability of the photocatalyst.

Keywords: Ni-CuWO₄/g-C₃N₄, photocatalysis, Z-scheme, nanocomposites, computational study

1. Introduction:

View Article Online
DOI: 10.1039/D0TA03729J

Photocatalytic organic transformations through semiconductor based nanocatalysts have recently gained very promising and challenging interest in the field of catalytic territory.¹⁻⁴ Photocatalytic hydroxylation of benzene to phenol is one of the most important reactions regarding this field. Benzene and phenol both act as very important intermediate in many chemical reactions.⁵ But being a polluting and carcinogenic, conversion of benzene to some other valuable chemicals is necessary for environmental benefit. Moreover, phenol is also a very important precursor or intermediate used for the synthesis of some pharmaceutical compounds, dyes, fibers, polymer resins, plastics etc.^{6,7} Phenol can also be used as intermediate in the synthesis of fungicides and can be used as a preservative.^{8,9} Phenol is mainly industrially prepared from benzene via three step cumene process.^{10,11} However, the yield of phenol is very low (only 5%) under this process which also requires high temperature and pressure in the presence of Lewis acid catalysts.^{12,13} These drawbacks lower the efficiency of cumene process, so, it is highly required to develop a new economic and environment friendly process for the production of phenol from benzene with high yield using homogeneous and heterogeneous catalysts.¹⁴⁻¹⁶

Catalytic aerobic oxidation of benzene to phenol in the liquid phase can be performed by using molecular oxygen as an oxidant. However, the requirement of sacrificial reducing agents such as hydrogen, CO, ascorbic acid and NADH analogues are the main drawback of this process.¹⁷⁻²¹ Because of this, oxidation system based on H₂O₂ as an oxidant has recently gained tremendous interest in catalytic oxidative process, as this process is green, economic and environment friendly and produces only water or dioxygen as products.²²

Development of a photocatalytic process using visible light as a source of light for the efficient conversion of benzene to phenol has drawn more concern in research field. Instead of using artificial source of light use of natural sunlight as an active source has earned great challenge in organic transformation reactions.²³ As most of the photocatalytic reactions are performed under conservative reaction conditions, developing a suitable photocatalyst which is of low cost and can be used to conduct the reactions under controlled reaction conditions with high phenol yield is very challenging.^{24,25} Many reports have been found to be articulated on visible light driven hydroxylation benzene to phenol using H₂O₂ as an oxidant.²⁶⁻³¹ Recently, Hutchings and co-workers have reported the photocatalytic oxidation of benzene to phenol under UV light using titania loaded monometallic Au and Pd as catalysts.³² Again, Hosseini et.al have reported the visible light oxidation of benzene to

phenol using bimetallic AuPd@g-C₃N₄ photocatalyst.²² Zhao et. al. has reported the g-C₃N₄ supported single metal atom catalyst for oxidation of benzene to phenol using H₂O₂.³³

Metal tungstates, MWO₄ (M=Ni, Cu, Fe, Mg etc.) with wolframite like structure, relatively high photocatalytic activity and good stability have recently attracted potential interest in photocatalytic reactions like CO₂ reduction, C-H activation and dye degradation etc.³⁴⁻³⁷ Recently, CuWO₄, a narrow band gap semiconductor has gained more importance as it can be used as photocatalyst in many reactions.^{38,39} However the photocatalytic performance of CuWO₄ is not that satisfactory due to the rapid recombination of photogenerated holes and electrons. The incorporation of other metal ions into CuWO₄ may able to enhance its photocatalytic activity. Nickel salts being cost effective and easily available, various forms of nickel can be used in many photocatalytic reactions. Again, considering the similar ionic radius with Cu²⁺, Ni²⁺ may easily replace Cu²⁺ ion in CuWO₄ crystal thereby improving its photocatalytic activity. Therefore, the first aim of this study is to develop a metal tungstate like CuWO₄ through the substitution of Ni²⁺ for better photocatalytic results.

Now-a-days, graphitic carbon nitride (g-C₃N₄), a 2D layered like semiconductor, has attracted enormous interest in photocatalysts because of its suitable band gap (2.7 eV) electronic structure, superior visible light response, high thermal stability and non-toxicity.⁴⁰ However, like other photocatalysts, the g-C₃N₄ has also encountered with high recombination of photogenerated holes and electrons which diminishes its photoactivity. To avoid this circumstances g-C₃N₄ has been blended with different narrow band gap materials to build a direct Z-scheme system for enhanced photocatalytic performance.⁴¹ Thus, the second aim of this work is to construct a novel g-C₃N₄ supported CuWO₄ nanocomposite through the substitution of Ni²⁺ (simply denoted as Ni-CuWO₄/g-C₃N₄) for efficient photocatalytic hydroxylation of benzene to phenol with high yield using natural sunlight as a promising source of light.

2. Experimental section:

2.1 Materials:

Urea (Himedia, 99.0%), CuCl₂.2H₂O (Sigma Aldrich, ≥ 99.0%), NiCl₂ (anhydrous, Alfa Aesar, 98.0%), polyethylene glycol 4000 (SRL), benzene (LobaCheme, 99.5%), phenol (Sigma Aldrich, ≥99.0%) chemicals were used for this research purpose. All the purchased chemicals are of analytical grade and were used directly without further treatment.

2.2 Catalyst preparation:

View Article Online
DOI: 10.1039/D0TA03729J

2.2.1 Synthesis of g-C₃N₄:

The bulk g-C₃N₄ was synthesized by thermal polymerisation of urea as reported earlier.⁴¹ Urea being less costly and easily available can be used as the most valuable precursor for the synthesis of g-C₃N₄. In a typical process, 20 g urea taken in a silica crucible covered with a lid was calcined in a muffle furnace at 550°C for 2 hrs with heating rate 5°C min⁻¹ under air atmosphere. After cooling to room temperature yellow coloured bulk g-C₃N₄ was formed as the desired product.

2.2.2 Synthesis of Ni-CuWO₄ (NCW):

Ni-CuWO₄ nanocompound can be synthesized by chemical precipitation method. In a typical synthesis, 1 mmol of CuCl₂.2H₂O was added to the solution of Na₂WO₄.2H₂O dissolved in 2% PEG-4000. A blue precipitate was found to be observed. After sonicated for half an hour, 1 mmol of NiCl₂ was added to it and mixed well. The blue precipitate turned bluish green after the addition of NiCl₂. After sonicated for half an hour, 1 mmol of NiCl₂ was added to it and mixed well. A bluish green precipitate was obtained. The mixture was then again sonicated in an ultrasonicator bath for 2 h and stirred for 6 h. The bluish green precipitate obtained was filtered and washed with deionized water followed by ethanol. The precipitate was dried under vacuum at 60°C and finally calcined at 500°C in a muffle furnace for 4 h to get the desired product.

2.2.3 Synthesis of Ni-CuWO₄/g-C₃N₄ nanocomposite (NCWCN):

For the synthesis of Ni-CuWO₄/g-C₃N₄ nanocomposite, the highly porous bulk g-C₃N₄ (340 mg) was first dispersed in 50 mL of methanol. Then the solution of g-C₃N₄ was ultrasonicated for almost 10 hrs for exfoliation. Subsequently, a certain amount of as prepared Ni-CuWO₄ (60 mg) was added to this solution and was sonicated for almost 5 hrs. The solution was then kept stirring for about 24 h. The product obtained was filtered and washed with distilled water followed by ethanol several times. Finally, the product was dried under vacuum at 60°C. The products obtained were labelled as x NCWCN, where x was denoted as the value of mass ratio of Ni-CuWO₄ and g-C₃N₄. Thus the as synthesized nanocomposite would contain mass ratio of 0.2. In this manner, different mass ratio containing Ni-CuWO₄/g-C₃N₄ such as 0.05, 0.1, 0.3, 0.4, 0.5 etc. nanocomposites were also synthesized. The percentage composition of main metal elements Cu, Ni, W in the catalysts

with different mass ratio were included in supporting information (Table S1). The synthesis method is represented in Figure 1.

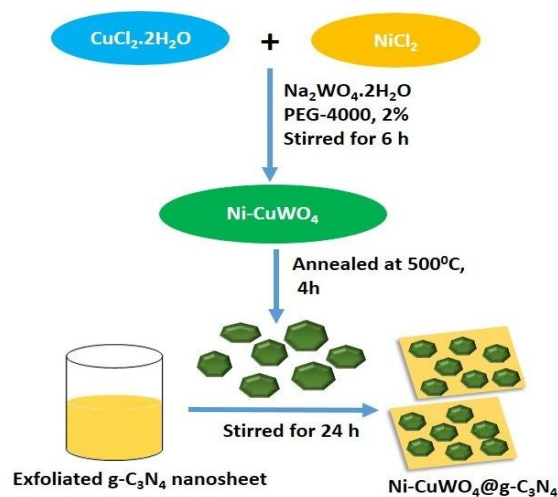
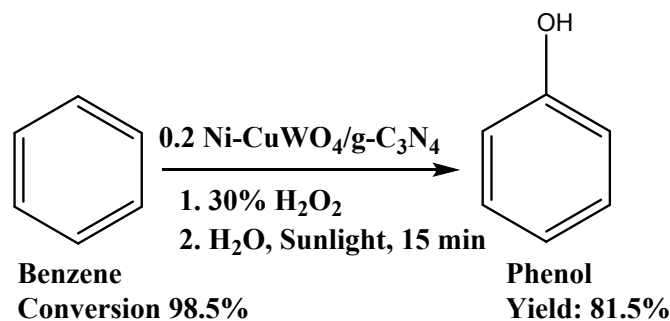


Figure 1. Synthesis of Ni-CuWO₄/g-C₃N₄

2.3 Activity test:

Catalytic experiments were done to investigate the activity of the photocatalysts for the conversion of benzene to phenol. In a typical procedure, 20 mg of prepared Ni-CuWO₄/g-C₃N₄ was taken in a 10 mL round bottom flask. To this 1 mL benzene and 200 μL distilled H₂O were added and the reaction mixture was stirred in dark for half an hour to establish adsorption-desorption equilibrium. 500 μL of 30% H₂O₂ was then added to the reaction mixture and was stirred in presence of sunlight. The reaction was stopped after a certain period of time and the catalyst was separated from the reaction mixture by centrifuge. The biphasic system appeared to be colourless before the reaction and it changed to light yellowish like colour in a single phase at the end of the reaction. The reactions were carried out on sunny days from 10 am to 12 pm with an intensity of about 160 watt/m². The liquid products were analysed by using GC 700 series (Thermo Scientific) equipped with a FID detector and capillary column (GC graph Figure S5). The GC oven temperature was set at 250°C for this sample and it was run for 4 mins. The required product was also further confirmed by doing ¹H NMR and ¹³C-NMR spectroscopy in a 500 MHz FT-NMR spectrometer (Figure S4). The reaction was performed with a series of catalyst of Ni-CuWO₄/g-C₃N₄ having different mass ratio of Ni-CuWO₄. But 0.2Ni-CuWO₄/g-C₃N₄ catalyst was found to give better result for this photocatalytic hydroxylation of benzene to phenol. The reaction pathway is shown in Scheme 1. The effects of reaction time, peroxide amount,

and light were also studied for this photocatalytic hydroxylation reaction by varying these parameters and keeping constant amount of benzene and aqueous medium. Some of the reactions were also carried out with molecular oxygen instead of using H_2O_2 under same reaction conditions to study their effects on the reaction by bubbling dioxygen (3 mL/min) to the bottom of the reaction mixture for 30 minutes before irradiation.



Scheme 1. Reaction pathway for photocatalytic hydroxylation of benzene to phenol

2.4 Catalyst characterisation:

The synthesized catalysts were characterised by PXRD (Powder X-ray Diffractometer), UV-Visible spectrophotometer, FTIR spectrometer, SEM (Scanning Electron Microscope), TEM (Transmission Electron Microscope), BET adsorption isotherm etc. The PXRD measurement was carried out on a Rigaku, ultima IV X-ray diffractometer of 2θ range $2-80^\circ$ using Cu $K\alpha$ -source of wavelength, $\lambda = 1.54 \text{ \AA}$. Nitrogen adsorption measurements were performed on Autosorb-iQ (Quantachrome USA) adsorption analyser which measures adsorption isotherm, specific surface area, pore volume mechanically. The samples were degassed at 250°C for 4 hrs. The FTIR spectra of the prepared catalysts were measured on SHIMADZU IR Affinity-1 spectrometer in the range of wave no $4000-400 \text{ cm}^{-1}$ using the KBr pellet technique. The UV-Visible spectroscopy of the synthesized catalysts was recorded on SHIMADZU UV-1800 spectrometer and the fluorescence spectroscopy was recorded on Horiba Scientific Fluorolog 3 spectrometer to generalise the optical properties. For analysing the surface, scanning electron microscopy images (SEM) were obtained Carl Zeiss SIGMA scanning electron microscope. The compositional analysis of the sample was performed by Energy Dispersive X-ray spectroscopy on Oxford EDS attached with the same instrument. TEM images were recorded on JEOL, JEM-2100 Plus Electron Microscope. XPS analysis was performed on an X-ray Photoelectron Spectrometer (ESCALAB Xi+, Thermo Fischer Scientific Pvt. Ltd., UK) using monochromatised $\text{AlK}\alpha$ radiation. The reaction products were analysed with a Trace GC 700 series GC system (Thermo Scientific) equipped with a FID detector and a capillary column.

The products formed were further confirmed by ^1H and ^{13}C NMR using 500 MHz FT-NMR spectrometer. View Article Online
DOI: 10.1039/D0TA03729J

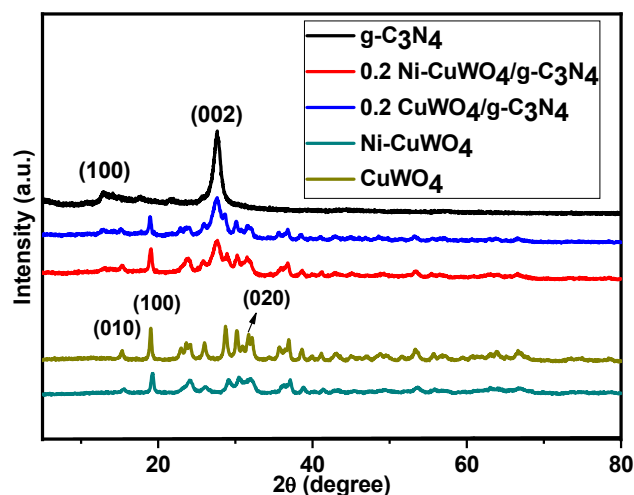
2.5 Computational Study

$3 \times \sqrt{3}$ and $\sqrt{3} \times 3$ single g- C_3N_4 layer containing 18 carbon and 24 nitrogen atoms were used to match a (3×2) twelve atomic layer stoichiometric CuWO_4 (010) surface slab containing 108 atoms of W, Cu and O atoms. Density functional calculations with hybrid functional PBE0 with relativistic small-core effective core-potential basis set of Stuttgart/Dresden (SDD) were used for all atoms using the periodic boundary condition as implemented in GAUSSIAN16 suite of program.⁴²⁻⁴⁴ The projected density of states (PDOS) were calculated on the optimized geometries using 128 k -space for the Brillouin zone interaction. Plots of the PDOS were obtained using a broadening energy parameter of 0.1 eV using Multiwfn program code.⁴⁵

3. RESULTS AND DISCUSSION

3.1 Catalyst characterisation:

The purity of phase and crystal structures of the as synthesized samples were analysed by powder XRD technique as shown in Figure 2. Two well-defined diffraction peaks are found in the samples, which are the characteristic peaks of typical g- C_3N_4 . The strongest peak at around 27.4° depicts a characteristic interlayer stacking structure of conjugated aromatic system triazine ring, indexes as the (002) crystal plane of the graphitic materials.⁴⁶ The small peak at 13.2° reflects the (100) plane of g- C_3N_4 . Again the observed diffraction peaks at 15.4° , 19° , 28.7° , 30.1° , 31.5° corresponding to the planes (010), (100), (-1-11), (111), (020) show the crystalline nature of CuWO_4 nanocompound confirming the formation of triclinic phase of CuWO_4 (JCPDS NO. 01-070-1732).⁴⁷ After the addition of Ni^{2+} species the intensity of the major diffraction peaks of CuWO_4 undergo a slight weakening and broadening due to incorporation of Ni^{2+} ion into CuWO_4 crystal replacing some of the Cu^{2+} ions during the synthesis process and thus implies that there is a close combination between Ni^{2+} species with CuWO_4 . The lattice parameters of composite 0.2 Ni- $\text{CuWO}_4/\text{g-C}_3\text{N}_4$ are also found to be less than that of 0.2 $\text{CuWO}_4/\text{g-C}_3\text{N}_4$ which may be due to substitution effect of Ni^{2+} into CuWO_4 .⁴⁸ Moreover with the increase in mass ratio of Ni- $\text{CuWO}_4/\text{g-C}_3\text{N}_4$ the intensities of the major diffraction peaks of g- C_3N_4 are also found to be diminished depicting the formation of nanocomposite with g- C_3N_4 (Figure S1).



View Article Online
DOI: 10.1039/D0TA03729J

Figure 2. PXRD pattern of as synthesized catalysts

For the further confirmation of the formation of nanocomposite FTIR spectra of g-C₃N₄, pure Ni-CuWO₄ and Ni-CuWO₄/g-C₃N₄ were studied and depicts in Figure 3. The intense band within 1230-1650 cm⁻¹ correspond to the typical stretching vibration mode of carbon nitride heterocycles.⁴⁹ The peak at 809 cm⁻¹ is associated with the characteristic mode triazine unit indicating the presence of typical structure of g-C₃N₄. The broad bands at 3020-3660 cm⁻¹ are the evidence of the presence of NH or NH₂ groups. For pure Ni-CuWO₄, the absorption band below 600 cm⁻¹ indicates the deformation modes of W-O-W bridges or W-O in the WO₄ tetrahedra.⁵⁰ The band appearing at around 1400 cm⁻¹ is associated with δ(OH) or ν_{W-O} bond.⁵¹ The bands around 700-800 cm⁻¹ can be attributed to the stretching of Cu-O bond.⁵⁰ From the figure it is seen that the intensity of the FTIR spectrum of the as synthesized Ni-CuWO₄/g-C₃N₄ is found to be slightly decreased compared to pure g-C₃N₄ which confirms that Ni-CuWO₄ nanocompound is chemically coordinated to the g-C₃N₄ support.

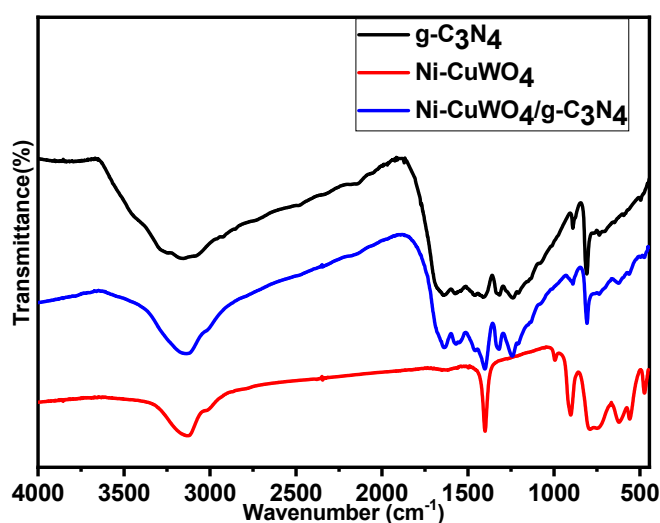
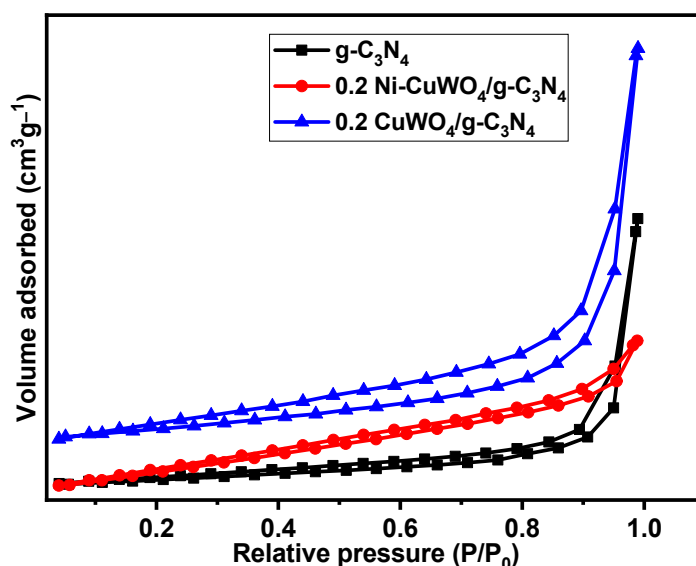


Figure 3. FTIR spectra of as synthesized catalystsView Article Online
DOI: 10.1039/D0TA03729J

The BET adsorption isotherm of pure g-C₃N₄, 0.2 Ni-CuWO₄/g-C₃N₄ and 0.2 CuWO₄/g-C₃N₄ catalysts are shown in the Figure 4. It is observed that pure g-C₃N₄ catalyst has a Brunauer-Emmet-Teller (BET) surface area of 50 m²g⁻¹ and a pore volume of 0.18 cm³g⁻¹, while the BET surface area of 0.2 Ni-CuWO₄/g-C₃N₄ and 0.2 CuWO₄/g-C₃N₄ are found to be 103.2 m²g⁻¹ and 81.6 m²g⁻¹ with pore volume 0.66 cm³g⁻¹ and 0.42 cm³g⁻¹ respectively (Table 1). The surface area of Ni-CuWO₄/g-C₃N₄ is found to be higher compared to CuWO₄/g-C₃N₄ and pure g-C₃N₄ implying that incorporation of Ni²⁺ into CuWO₄ leads to increase in surface area of Ni-CuWO₄. The increase in surface area of Ni-CuWO₄/g-C₃N₄ with respect to bare support is due to doping effect and the creation of new pores due to an effective diffusion of Ni-CuWO₄ species in the g-C₃N₄ support during the preparation method which causes increase in surface roughness without clogging pores.⁵²

**Figure 4.** Nitrogen adsorption-desorption isotherms of the as prepared samples.**Table 1.** BET surface area analysis of the synthesized catalysts

Catalyst	BET surface area (m ² g ⁻¹)	Pore volume (cm ³ g ⁻¹)	Pore radius (nm)
g-C ₃ N ₄	50.2	0.18	1.8
0.2 CuWO ₄ /g-C ₃ N ₄	81.6	0.42	1.9
0.2 Ni-CuWO ₄ /g-C ₃ N ₄	103.2	0.66	1.9

Figure 5a illustrates the UV-Visible absorption abilities of pure g-C₃N₄, 0.2 NiWO₄/g-C₃N₄, 0.2 CuWO₄/g-C₃N₄, pure Ni-CuWO₄ and 0.2 Ni-CuWO₄/g-C₃N₄ composites. From the Figure 5a it is observed that pure g-C₃N₄ possesses a blue shifted absorption edge at around

450 nm which is associated to the $n-\pi^*$ electronic transition of lone pair electrons of N-atoms.³⁵ It can be observed that the UV-Visible absorption capacity of the as prepared composites are higher than that of pure $g-C_3N_4$. The energy band gaps of the synthesized materials estimated via a Tauc plot based on UV-Visible absorption results are shown in the Figure 5b. The Tauc plot is based on the following formula:

$$\alpha h\nu = A(h\nu - E_g)^{n/2}$$

Where α is the absorption coefficient, h is the Planck's constant, A is a constant, ν is the frequency of light, E_g is band gap energy, and the n value is determined by the type of optical transition of semiconductor ($n=1$ and 4) with direct or indirect band characteristics.⁵³ The energy gap of the composite $Ni-CuWO_4/g-C_3N_4$ (2.2 eV) is found to be narrower than that of composite $CuWO_4/g-C_3N_4$ (2.5 eV) as evident from the Figure 5b. The incorporation of Ni^{2+} ion into $CuWO_4$ crystal may affect the band edge positions of $CuWO_4$ i.e. top of CB and bottom of VB helping in generating an intermediary level between CB and VB of the $CuWO_4/g-C_3N_4$ which causes decrease in band gap of $Ni-CuWO_4/g-C_3N_4$ and enhances its visible light absorption capacity.⁵⁴ Owing to narrow band gap energy the photocatalysts $Ni-CuWO_4$ and $g-C_3N_4$ upon irradiation of sunlight absorbs incident visible light which helps in transfer of electron from VB to CB creating holes in its VB. As a Z-scheme material, the photoinduced electrons in the CB of $Ni-CuWO_4$ tends to recombine with the photogenerated holes in the VB of $g-C_3N_4$ maintaining electron in the CB of $g-C_3N_4$ and holes in the VB of $Ni-CuWO_4$. This process helps in minimizing the fast recombination of electron and hole pairs which intensifies the optical property of Z-scheme narrow band gap semiconductor composites like $Ni-CuWO_4/g-C_3N_4$.

The photoluminescence property of the synthesized materials $g-C_3N_4$, $0.2 NiWO_4/g-C_3N_4$, $0.2 CuWO_4/g-C_3N_4$ and $0.2 Ni-CuWO_4/g-C_3N_4$ composites are shown in the Figure 5c. A compound having a lower PL intensity helps in better charge separation of photoinduced holes and electrons which is observed from the Figure 5c.³⁵ The $g-C_3N_4$ has a strong emission peak at around 450 nm indicating that there is fast recombination of photogenerated holes and electron pairs in $g-C_3N_4$ which lowers its photoactivity to some extent. On the other hand, it can be said that combination of $g-C_3N_4$ with other material by forming a heterojunction helps in enhancing the charge separation efficiency of photogenerated holes and electrons. Again, the PL intensity of composite $0.2 Ni-CuWO_4/g-C_3N_4$ is found to be the least amongst the all composites like $0.2 CuWO_4/g-C_3N_4$, $0.2 NiWO_4/g-C_3N_4$. This may be due to substitution of

Ni^{2+} into CuWO_4 which helps in creating an intermediary level between CB and VB of CuWO_4 thus minimizing the recombination process of electron and hole pairs of the material $\text{Ni-CuWO}_4/\text{g-C}_3\text{N}_4$ and enhanced its photocatalytic activity.

To further investigate the charge transfer properties of the as synthesized materials, time resolved PL spectra of pure $\text{g-C}_3\text{N}_4$ and the composite $0.2 \text{ Ni-CuWO}_4/\text{g-C}_3\text{N}_4$ were also performed and is depicted in Figure 5d. Generally, the shorter the life time, faster is the recombination of photogenerated electron and hole pairs; on the contrary, longer life time is associated with the lower recombination i.e. fast separation of electron-hole pairs.⁵⁵ It is observed from the decay curves that the composite $0.2 \text{ Ni-CuWO}_4/\text{g-C}_3\text{N}_4$ had longer life time compared to its support $\text{g-C}_3\text{N}_4$. The reason for prolonged life time of the composite may be due to interfacial electron transfer with $\text{g-C}_3\text{N}_4$ indicating the formation of heterojunction with $\text{g-C}_3\text{N}_4$ thereby improving its photocatalytic activity.

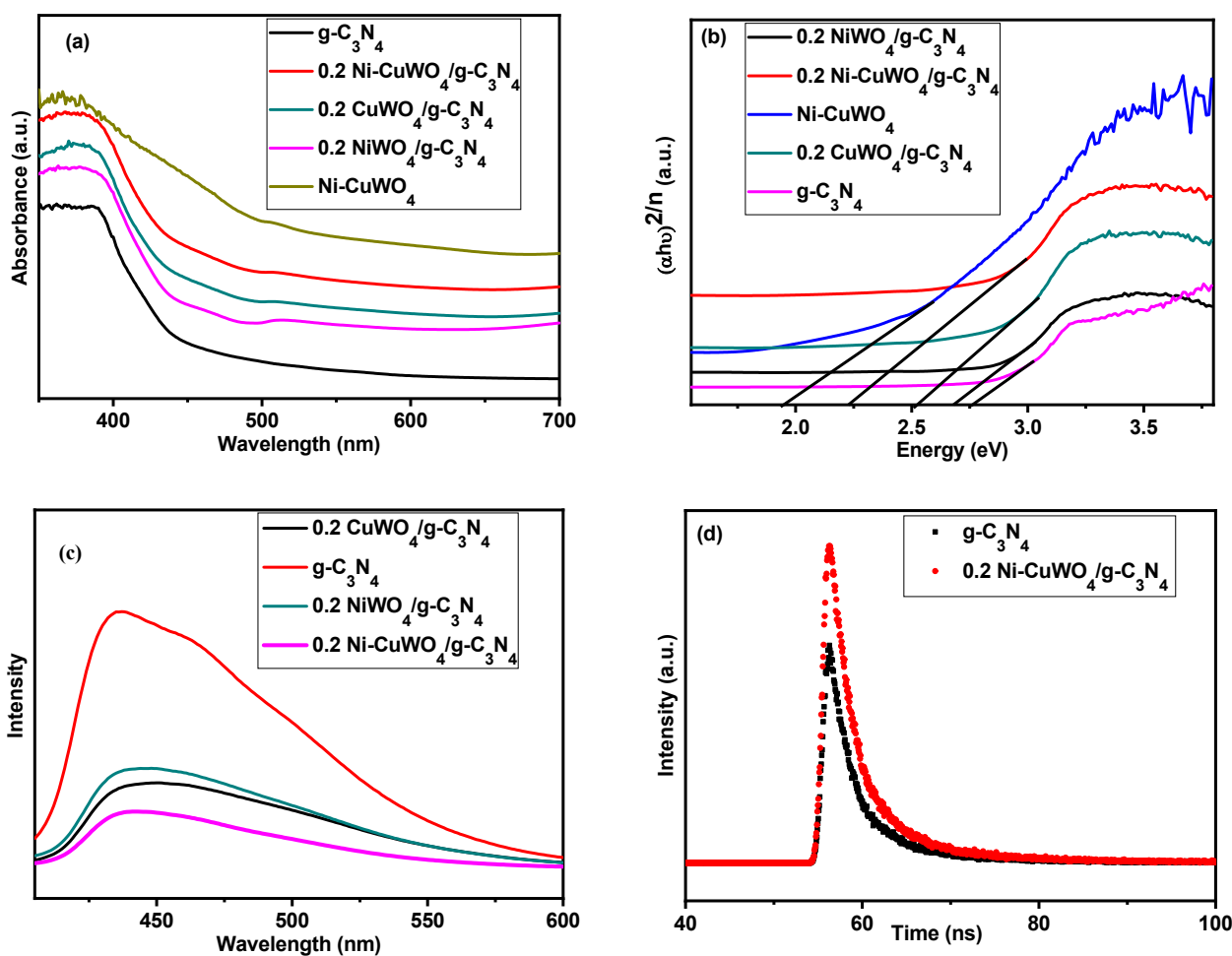


Figure 5.(a) UV-DRS spectra, (b) Tauc plot, (c) PL spectra and (d) life time spectra of as synthesised catalysts.

The thermal stability of the synthesized materials $g\text{-C}_3\text{N}_4$ and $0.2 \text{ Ni-CuWO}_4/g\text{-C}_3\text{N}_4$ was examined by thermogravimetric analysis (TGA) under N_2 atmosphere with a heating rate of $10^\circ\text{C}/\text{min}$ at temperature range ambient to 800°C (Figure 6). The $g\text{-C}_3\text{N}_4$ is stable up to 550°C under N_2 atmosphere and rapid weight loss of the material is observed 550°C which can be attributed to the decomposition of $g\text{-C}_3\text{N}_4$. On the other hand, the composite $0.2 \text{ Ni-CuWO}_4/g\text{-C}_3\text{N}_4$ shows its thermal stability up to 490°C which is lower than that of pure $g\text{-C}_3\text{N}_4$. The initial decomposition of the composite starts at 490°C and the complete decomposition occurs at 615°C indicating the combustion of $g\text{-C}_3\text{N}_4$ in the composite under N_2 atmosphere. The residual content of Ni-CuWO_4 in the composite $\text{Ni-CuWO}_4/g\text{-C}_3\text{N}_4$ can be easily calculated from the weight remainder after heating the sample up to 800°C and is found to be $\sim 9.8\%$. This may be due to the absorption and activation of atmospheric oxygen on the catalyst considering the oxidative property of the material.⁵⁶

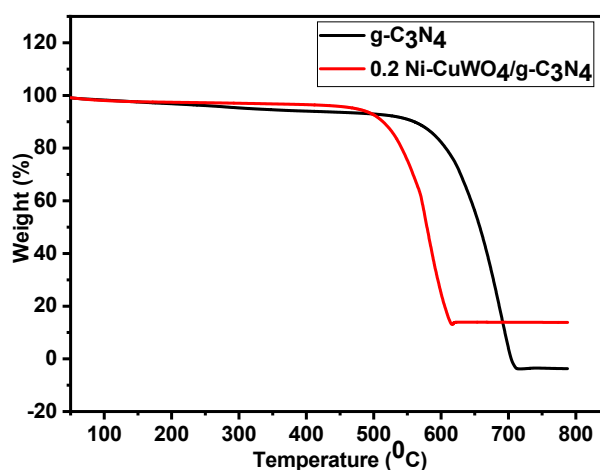


Figure 6. TGA curves of pure $g\text{-C}_3\text{N}_4$ and composite $0.2 \text{ Ni-CuWO}_4/g\text{-C}_3\text{N}_4$

The as synthesized $0.2 \text{ Ni-CuWO}_4/g\text{-C}_3\text{N}_4$ was further investigated by XPS analysis, which is shown in Figure 7. The XPS data shows the presence of C, N, O, Cu, Ni and W on the surface of the catalyst and their concentration were 42.1%, 41.8%, 11.5%, 1.7%, 1.1% and 1.8% respectively. The photoelectron peaks of these elements are distinctly observed from the XPS spectra at binding energies of 286.9 eV (C1s), 398.1 eV (N1s), 530.2 eV (O1s), 935.1 eV (Cu2p), 874.8 eV (Ni2p) and 35.4 eV (W4f) respectively (Figure 7a). The high resolution C1s spectra (Figure 7b) can be fitted into several C species with different binding energies of 283.7 eV and 287.1 eV, corresponding to graphitic carbon (C-C) and sp^2 -bonded carbon (N-C=N) respectively.⁵⁷ The high resolution N1s spectra (Figure 7c) for $0.2 \text{ Ni-CuWO}_4/g\text{-C}_3\text{N}_4$ exhibits three N states including triazine rings, C=N-C (397.5 eV), tertiary

nitrogen, N-(C)₃ (399.3 eV) and the amino functions, N-H (402.8 eV) which are the three units that constituted the heptazine ring of g-C₃N₄.⁵⁸ It infers that the framework of g-C₃N₄ is not altered with the loading of Cu, Ni and tungsten species. There are two main peaks of O1s with binding energies of 529.5 eV, 531.4 eV and 533.1 eV as shown in Figure 7d. The peak at 529.5 eV can be assigned to the lattice oxygen of Ni-CuWO₄. Another peak at 531.4 eV indicates the presence of oxygen vacancies in the photocatalyst and the peak at 533.1 eV corresponds to the oxygen of -OH in water molecules which may be due to loosely bound moisture on the surface of the solid.⁵⁹ The higher resolution Cu2p XPS spectra are shown in Figure 7e. The Cu2p_{3/2} and Cu2p_{1/2} are observed at 933.4 eV and 953.2 eV respectively and these doublet peaks with ratio 1:2 are occurred due to spin orbit coupling. Because of the inelastic scattering of the core level electrons strong shake-up peaks are observed at 940.1 eV and 942.4 eV for Cu2p_{3/2} and another one at 962.0 eV for Cu2p_{1/2} implying the presence of Cu²⁺ species in the composite.⁶⁰ As shown in Figure 7f, the Ni2p spectra mainly depicts the peaks of Ni2p_{3/2} and Ni2p_{1/2} orbits owing to spin orbit coupling at binding energies of 855.2 eV and 873.4 eV respectively, as well as two shake-up satellite peaks mainly indicating the presence of Ni²⁺ species.⁶¹ The deconvoluted high resolution XPS spectra of W4f (Figure 7g) shows two main peaks of W4f at 34.5 eV and 36.4 eV correspond to W4f_{7/2} and W4f_{5/2} respectively as well as two satellite peaks at 35.4 eV for W4f_{7/2} orbit and 37.5 eV for W4f_{5/2} confirming the presence of tungsten in W⁶⁺ state.⁶²

New Article Online
DOI: 10.1039/D0TA03729J

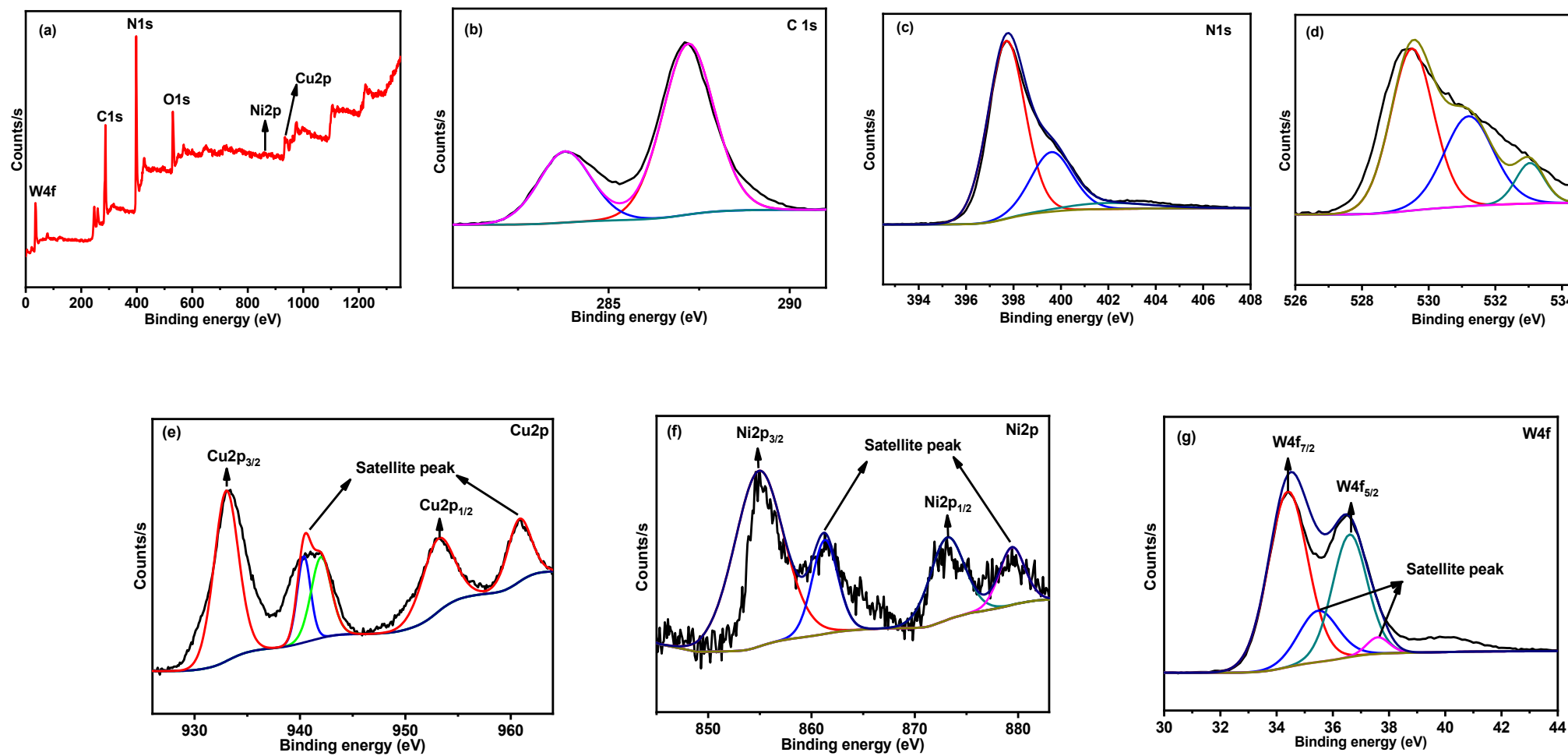


Figure 7.(a) XPS survey, (b) C1s XPS spectra, (c) N1s XPS spectra, (d) O1s XPS spectra, (e) Cu2p XPS spectra, (f) Ni2p XPS spectra and (g) W4f XPS spectra of catalyst 15% Ni-CuWO₄/g-C₃N₄

Morphological structures of pure $g\text{-C}_3\text{N}_4$ and $0.2 \text{ Ni-CuWO}_4/g\text{-C}_3\text{N}_4$ are further verified by SEM, TEM and HRTEM analysis. The SEM image of pure $g\text{-C}_3\text{N}_4$ sample shows closely arranged staking of the conjugated aromatic system with some small scattered particles at the surface which is depicted in the inset of Figure 8a. The reason may be due to the light layer crack during the crystal growth.⁶³ Figure 8b showed the Ni-CuWO_4 particles appears as clusters having polyhedral shapes. The elemental composition of this nanocomposite is obtained from the EDX pattern of $0.2 \text{ Ni-CuWO}_4/g\text{-C}_3\text{N}_4$ which confirms the presence of C, N, O, Cu, Ni & W in the compound (Figure 8c). The TEM, HRTEM images of the pure $g\text{-C}_3\text{N}_4$ and synthesized $0.2 \text{ Ni-CuWO}_4/g\text{-C}_3\text{N}_4$ are shown in Figure 8d, 8e & 8f. Figure 8d shows a TEM image of the synthesized pure $g\text{-C}_3\text{N}_4$ nanosheets. It is observed that the TEM image showed free standing nanosheets with diameters of few nanometres. Figure 8e shows an enlarged image of the composite $0.2 \text{ Ni-CuWO}_4/g\text{-C}_3\text{N}_4$. Uniform distribution of supported Ni-CuWO_4 nanoparticles having polyhedral morphology was seen in the TEM image. The HRTEM images of $\text{Ni-CuWO}_4/g\text{-C}_3\text{N}_4$ along with pure $\text{CuWO}_4/g\text{-C}_3\text{N}_4$ are also depicted in Figure 8f and 8g. It can be observed from the HRTEM images that the lattice spacing of (010) plane of CuWO_4 in the $\text{Ni-CuWO}_4/g\text{-C}_3\text{N}_4$ nanocomposite is somewhat different from that of pure $\text{CuWO}_4/g\text{-C}_3\text{N}_4$. This is because of the incorporation of Ni^{2+} into CuWO_4 crystal leading to disorder in the crystal. Besides this the HRTEM images also revealed an integration heterojunction of $\text{Ni-CuWO}_4/g\text{-C}_3\text{N}_4$ or $\text{CuWO}_4/g\text{-C}_3\text{N}_4$ which enabled the formation of Z-direct scheme enhancing the photocatalytic performance by preventing the charge recombination of these materials. Furthermore, the selected area electron diffraction (SAED) pattern is also shown in the inset of Figure 8f. The diffused rings in the SAED pattern implied the formation of crystalline phases over the support due to interaction of Ni-CuWO_4 nanoparticles with the $g\text{-C}_3\text{N}_4$ support. The STEM image of the composite $0.2 \text{ Ni-CuWO}_4/g\text{-C}_3\text{N}_4$ is also shown in Figure 8h and EDX mapping images of composite $0.2 \text{ Ni-CuWO}_4/g\text{-C}_3\text{N}_4$ are depicted in Figure 9a-9f which also confirmed the existence of C, N, O, Cu, Ni and W elements in the composite. The presence of lower content of Cu, Ni and W elements in the composite can be ensured from the low intensity signal of these elements.

View Article Online
DOI: 10.1039/D0TA03729J

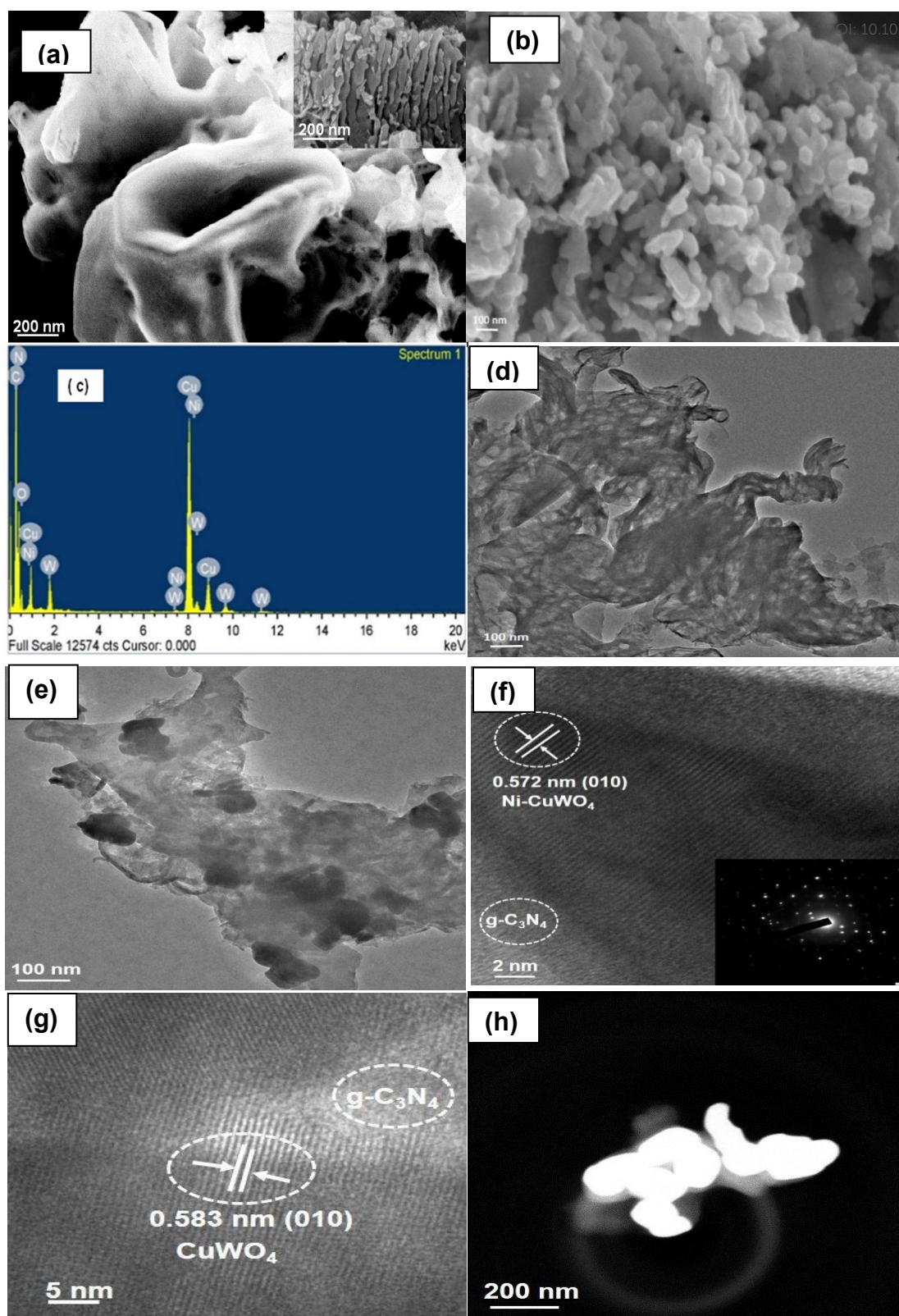


Figure 8. (a), (b) FESEM images of $g\text{-C}_3\text{N}_4$ and Ni-CuWO_4 respectively, (c) EDX pattern of composite 0.2 NCWCN, (d) and (e) TEM images of $g\text{-C}_3\text{N}_4$ and the composite 0.2 NCWCN respectively, (f) and (g) HRTEM images of 0.2 NCWCN and 0.2 CWCN respectively, (h) STEM image of composite 0.2 $\text{Ni-CuWO}_4/g\text{-C}_3\text{N}_4$

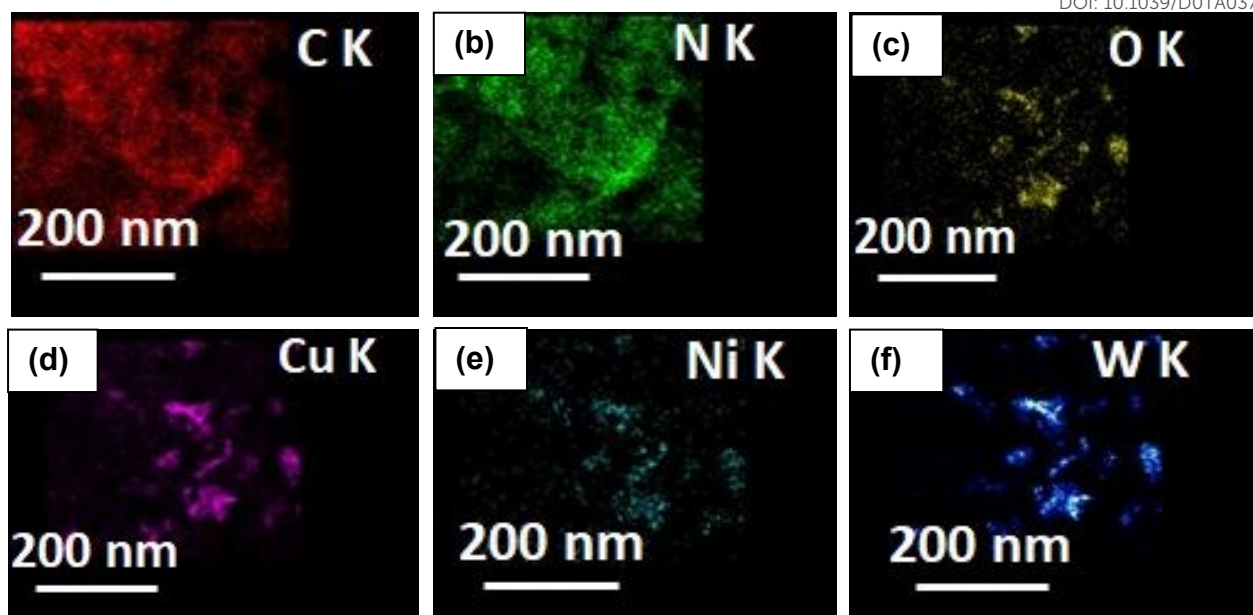


Figure 9. (a) to (f) elemental mapping of composite 0.2 Ni-CuWO₄/g-C₃N₄

3.3. Catalyst screening for photocatalytic hydroxylation of benzene to phenol:

3.3.1 Effect of metal loading:

The activity of the as synthesized catalysts were investigated for the photocatalytic hydroxylation of benzene to phenol under sunlight irradiation using H₂O₂(30% V/V) as an oxidant in aqueous medium. The results are summarized in Table 2. The amount of benzene was kept constant in all the reactions.

As predicted no benzene conversion is observed when the reaction was carried out without any catalyst (entry 1). With pristine Ni-CuWO₄ (NCW) 25.8% benzene conversion was observed (entry 7). Again with pure g-C₃N₄ very poor conversion of benzene was obtained with low yield of phenol (entry 10). In contrast, when the hydroxylation reaction was conducted with g-C₃N₄ supported Ni-CuWO₄ (Ni-CuWO₄/g-C₃N₄) having different mass ratio of Ni-CuWO₄/g-C₃N₄, an increase in the conversion of benzene was observed (entries 2-6). With 0.05 Ni-CuWO₄/g-C₃N₄, 68.7% conversion of benzene is obtained with 70.2% selectivity of phenol. However, the yield of phenol is not satisfactory (48.2%). The low yield of phenol is observed because of the lower conversion of benzene and this may be due to presence of less amount of active catalytic sites in the 0.05 mass ratio of Ni-CuWO₄/g-C₃N₄. But, it is observed that with the increase in the mass ratio of Ni-CuWO₄/g-C₃N₄ from 0.1-0.4

the conversion of benzene is also found to be enhanced from 82.6% to >99% (Table 1, entries 3-6).

Table 2. Photocatalytic hydroxylation of benzene to phenol over various catalysts^a

Entry	Catalyst	Benzene conversion (%)	Phenol selectivity (%)	Phenol yield (%)
1	No catalyst	0	0	0
2	0.05 NCWCN	68.7	70.2	48.2
3	0.1 NCWCN	82.6	75.3	62.2
4	0.2 NCWCN	98.5	82.7	81.5
5	0.3 NCWCN	>99	74.5	73.2
6	0.4 NCWCN	>99	60.6	60.3
7	Ni-CuWO ₄	25.8	62.5	16.1
8	0.2 NWCN	30.2	54.5	16.5
9	0.2 CWCN	32.5	56.3	18.3
10	g-C ₃ N ₄	≈2	<1	-----
11 ^b	0.2 NCWCN	16.8	94.3	15.8
12 ^b	Ni-CuWO ₄	4.8	95.2	4.5
13 ^b	g-C ₃ N ₄	≈1	-----	-----

^aReaction conditions: catalyst (20 mg), benzene (1 mL, 11.3 mmol), H₂O (0.2 mL), H₂O₂ (0.5 mL), reaction time (15 min), sunlight, ^breactions performed with molecular oxygen

The best result is observed with 0.2 Ni-CuWO₄/g-C₃N₄ which provided 98.5% conversion of benzene with 82.7% selectivity and 81.5% yield of phenol for 15 minutes of reaction under sunlight and is worth mentioning. However, with the increase in the mass ratio of the composite Ni-CuWO₄/g-C₃N₄ up to 0.4 a decrease in selectivity and yield of phenol are found to be attained (entry 5, 6). This may be due to increase in the active catalytic sites with the increase in the mass ratio of Ni-CuWO₄/g-C₃N₄ produces more hydroxyl radicals. This enables more benzene conversion and produced phenol, but the presence of excess amount hydroxyl radicals further oxidizes phenol and produces other product like p-Benzoquinone. Again with individual NiWO₄/g-C₃N₄ (0.2 NWCN) and CuWO₄/g-C₃N₄ (0.2 CWCN), lower benzene conversion with low phenol yield are obtained (entries 8, 9). Thus Ni-CuWO₄/g-C₃N₄ (0.2 mass ratio of Ni-CuWO₄/g-C₃N₄) is found to be the best catalyst for conversion of benzene to phenol with high yield and this may be due to the incorporation of Ni²⁺ ions into

CuWO₄ crystal which leads to increase in the active catalytic sites in the composites, for photocatalytic performance. View Article Online
DOI: 10.1039/D0TA03729J

3.3.2 Effect of catalyst amount:

The effect of 0.2 Ni-CuWO₄/g-C₃N₄ catalyst amounts on the sunlight driven hydroxylation of benzene to phenol is also surveyed and the results are depicted in Figure 10a. When the reaction is carried out with 10 mg of catalyst 72.4% conversion of benzene with 92.5% selectivity and 67% yield of phenol are found to be observed. With the increase of catalyst amount upto 30 mg a gradual increment the conversion of benzene is observed and with 20 mg of catalyst the reaction shows its best result of 98.5% conversion of benzene with 81.5% yield of phenol. However, further increasing the catalyst amount upto 30 mg a decrease in the yield of phenol is observed. This is because of the formation of other product like p-benzoquinone by the over oxidation of phenol. It can be narrated that with the increase in catalyst amount in the reaction mixture would lead to increase in the active catalytic sites which produced more hydroxyl radicals. This enhances the conversion of benzene molecules and produces phenol, but the presence of excess amount hydroxyl radicals accelerates the over oxidation of phenol and produces other product like p-benzoquinone. Thus 20 mg of catalyst amount is found to be the appropriate amount for the production of high yield of phenol.

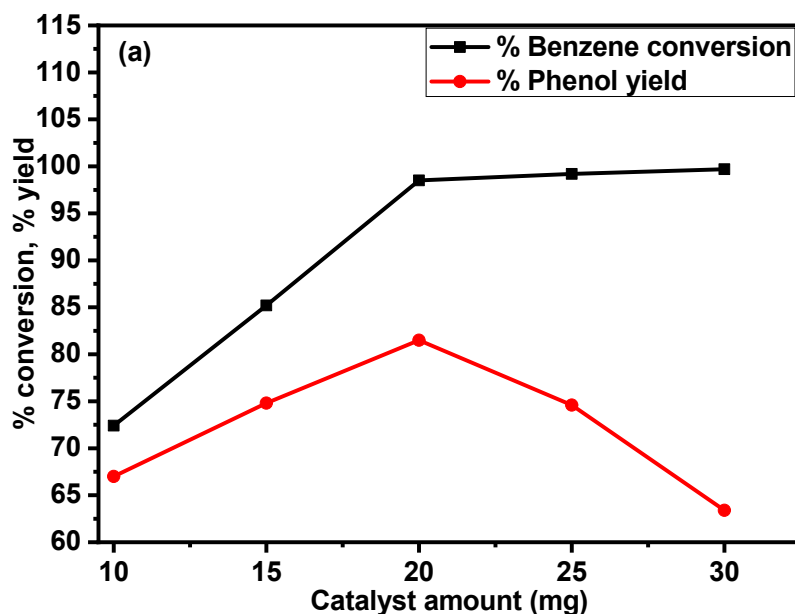


Figure 10a. Effect of catalyst amount in photocatalytic hydroxylation of benzene to phenol under sunlight irradiation. Reaction conditions: catalyst from 10 mg to 30 mg, benzene (1 mL, 11.3 mmol), H₂O (0.2 mL), H₂O₂ (0.5 mL), reaction time (15 min), sunlight

3.3.3 Effect of reaction time:

View Article Online
DOI: 10.1039/D0TA03729J

Reaction time has significant influence on photocatalytic hydroxylation of benzene to phenol and this is depicted in Figure 10b. It is clear from the figure that a lower benzene conversion of 25.6% is observed with high selectivity of phenol, 95.2% when the reaction is carried out for five minutes under natural sunlight. The low conversion also affects the yield of phenol and was found to be a bit low (24.3%). However, with the subsequent increase in time from 10 minutes to 60 minutes, conversion of benzene is also found to be boosted from 60.2% to >99% with increase in phenol yield upto 15 minutes. However the selectivity of phenol is observed to be low and the reaction reaches its optimization condition with 98.5% conversion of benzene and 82.7% selectivity and 81.5% yield of phenol after 15 minutes of reaction. It is observed that with gradual increase in time yield of phenol is also found to be diminished. This is due to more exposure to sunlight with increase in time which causes more H_2O_2 decomposition and produces more hydroxyl radicals and because of the surplus amount of hydroxyl radicals some of phenol produced in the reaction gets over oxidized and produces other hydroxylated benzene product. Thus these results indicate that phenol is more stable under our optimized reaction condition i.e. for 15 minutes of reaction.

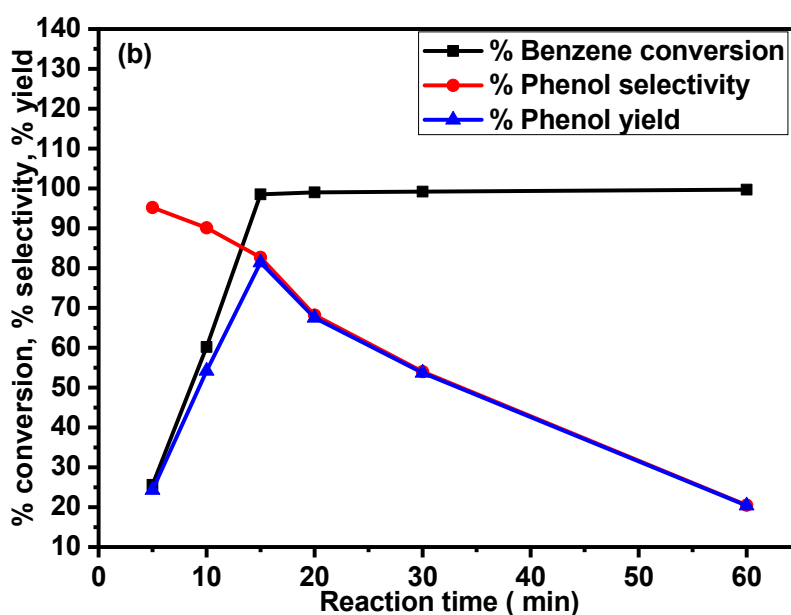
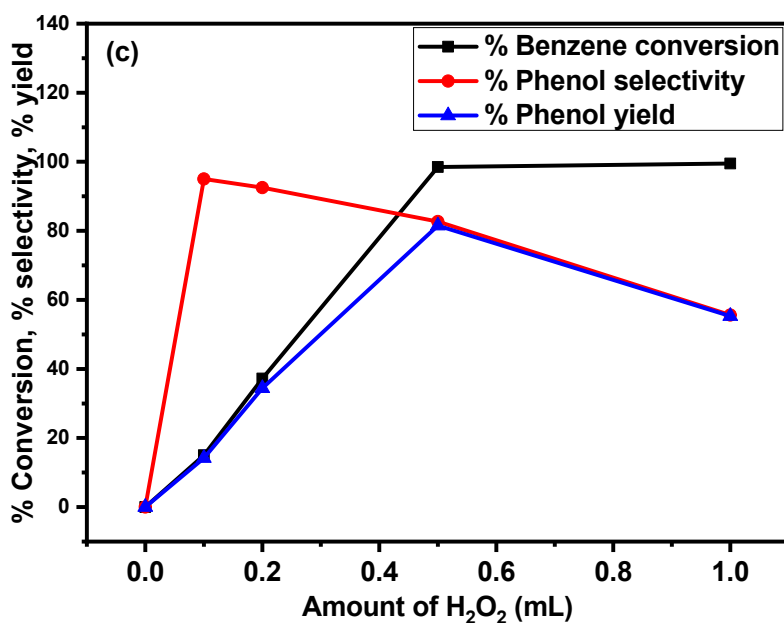


Figure 10b. Effect of catalyst amount in photocatalytic hydroxylation of benzene to phenol under sunlight irradiation. Reaction conditions: catalyst (20 mg), benzene (1 mL11.3 mmol), H_2O (0.2 mL), H_2O_2 (0.5 mL), reaction time from 5 to 60 minutes, sunlight

3.3.4 Effect of H₂O₂ and molecular oxygen:

The effect of H₂O₂ in hydroxylation of benzene to phenol is also studied and this is summarized in Figure 10c. It is observed that without H₂O₂ there is no benzene conversion within 15 minutes. With lower amount of H₂O₂ (30% V/V) such as 100 μL, very low conversion of benzene (15%) is observed with 95% selectivity of phenol. However, the yield of phenol is not convincing (only 14.2%). When the reaction was carried out for 1h the conversion was found to be increased to around 80.5% with phenol yield of 67.2%. With the increase in the peroxide amount from 200 μL to 1000 μL gradual enhancement in the conversion of benzene is marked upto >99%, but with a decrease in selectivity from 92.5% to 55.6%. The reaction shows its better result with 500 μL of H₂O₂ and is found to be optimized with 98.5% conversion of benzene and with 81.5% phenol yield. The increase in phenol yield with the increase in the amount of peroxide upto 500 μL is the indication of the presence of more hydroxyl radicals in the reaction mixture. These hydroxyl radicals lead to more benzene conversion by attacking benzene rings and produce more hydroxylated species of benzene like phenol. However, when the peroxide amount is increased upto 1000 μL a decline in the yield of phenol is happened to be noticed although the conversion of benzene is remarkably high. This is because of the formation of other hydroxylated product p-Benzoquinone due to over oxidation of phenol. Thus, it is worth mentioning that H₂O₂ has significant effects on hydroxylation of benzene to phenol. The results of the reactions which were carried out with molecular oxygen (dioxygen, O₂) are illustrated in Table 2 (entries 11-13). It is observed from the results that there is about 16.8% conversion of benzene with 0.2NCWCN photocatalyst for 15 minutes of reaction (Table 2, entry 11) and the phenol yield is also in the lower side. This can be explained on the basis of oxidising property of molecular oxygen. Molecular oxygen is not as strong as H₂O₂ as an oxidising agent because of its lower reduction potential as compared to H₂O₂. Additionally, molecular oxygen needs to form first H₂O₂ to achieve the desired product phenol by capturing electron from the photocatalyst in a prolonged way as discussed in the reaction mechanism (Figure 11b) thereby explaining the role of oxygen in this photocatalytic hydroxylation.



View Article Online
DOI: 10.1039/D0TA03729J

Figure 10c. Effect of peroxide amount in photocatalytic hydroxylation of benzene to phenol under sunlight irradiation. Reaction conditions: catalyst (20 mg), benzene (1 mL, 11.3 mmol), H₂O (0.2 mL), H₂O₂ from 0.1 mL to 1 mL, reaction time (15 min), sunlight

3.3.5 Effect of light:

To study the effects of light some of the reactions were also executed in dark along with sunlight irradiation. It is accessed from the GC results that no noticeable conversion of benzene as well as phenol yield is obtained when the reactions are performed under dark (Table 3, entries 1-5). The catalytic activity is found to be remarkably intensified with exposure to sunlight. It is also monitored from the results that in dark only 2.4% conversion of benzene is obtained with catalyst 0.2 Ni-CuWO₄/g-C₃N₄ under optimised reaction conditions (entry 3). The hydroxylation process seems to be enhanced with 98.5% conversion of benzene when the reaction is performed in presence of sunlight irradiation. Under sunlight irradiation the catalysts adsorbs sunlight and stimulates the decomposition of H₂O₂. Consequently, large no. of hydroxyl radicals are generated which attack benzene molecules and convert to phenol and other hydroxylated products. Thus it can be implied that light has compelling influence in this hydroxylation reaction.

Table 3. Effect of light in photocatalytic hydroxylation of benzene to phenol over various catalysts^a

View Article Online
DOI: 10.1039/D0TA03729J

Entry	Catalyst	In sunlight		Under dark
		Benzene conversion (%)	Phenol yield (%)	Benzene conversion (%)
1	g-C ₃ N ₄	≈2	<1
2	Ni-CuWO ₄	25.8	16.1	<1
3	0.2 NCWCN	98.5	81.5	≈2.4
4	0.2 CWCN	32.5	18.3	<2
5	0.2 NWCN	30.2	16.5	≈1

^aReaction conditions: catalyst (20 mg), benzene (1 mL, 11.3 mmol), H₂O (0.2 mL), H₂O₂ (0.5 mL), reaction time (15 min), reactions were performed under both sunlight and dark

3.3.6 Plausible reaction mechanism:

For mechanistic investigation, a series of trapping experiments were performed to explore the effects of active species including ·OH, h⁺ and e⁻ in the photocatalytic process. Therefore, three different chemicals were chosen as scavengers for these trapping experiments and these were isopropanol for ·OH, EDTA for h⁺ and K₂Cr₂O₇ for e⁻.

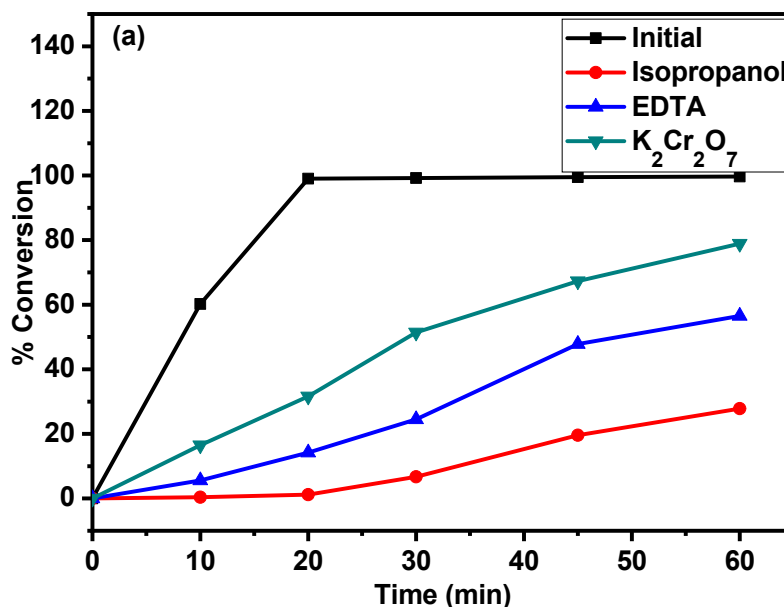


Figure 11a. Photocatalytic hydroxylation of benzene to phenol with or without scavengers.

^aReaction conditions: catalyst (20 mg), benzene (1 mL, 11.3 mmol), H₂O (0.2 mL), H₂O₂ (0.5 mL), reaction time (15 min), scavengers (20 mmol).

From the results depicted in Figure 11a it is observed that when isopropanol and EDTA are used in the reaction system there is significant quenching in the photocatalytic activity, indicating that $\cdot\text{OH}$ and h^+ are the main active species. Thereby comparing the conversion of benzene after inclusion of these scavengers the significance of these three types of species follows a trend of $\cdot\text{OH} > \text{h}^+ > \text{e}^-$.

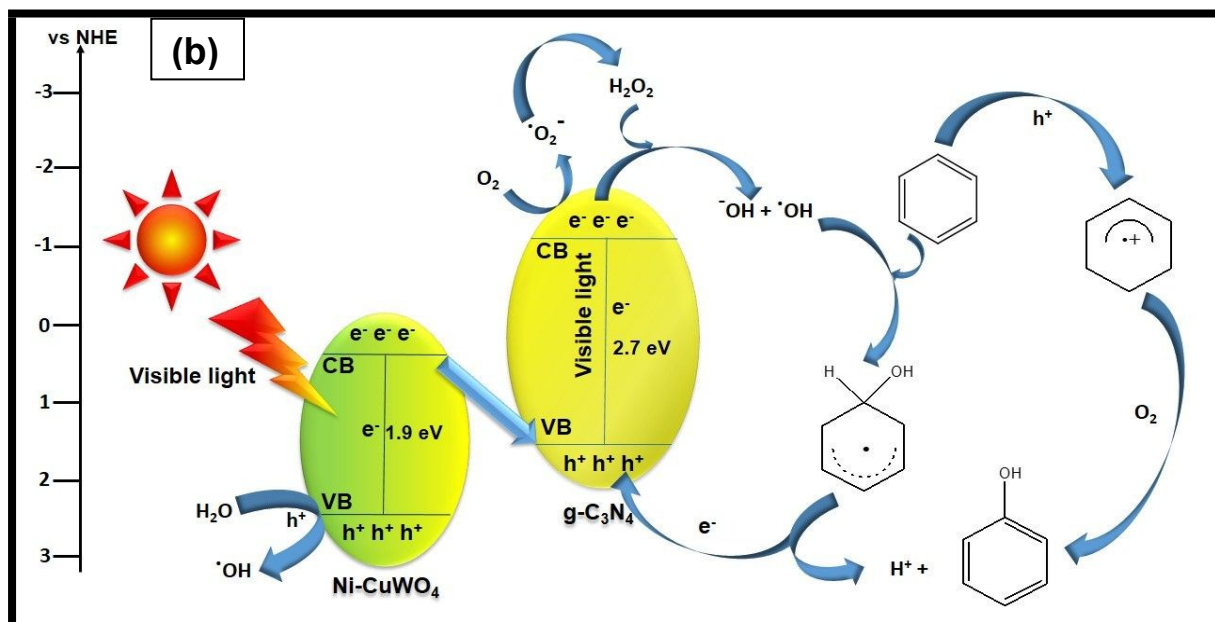


Figure 11b. Plausible mechanism of photocatalytic hydroxylation of benzene to phenol

Based on these results, a Z-scheme photocatalytic mechanism for Ni-CuWO₄@g-C₃N₄ nanocomposite can be proposed and schematically depicts in Figure 11b. Under sunlight irradiation both Ni-CuWO₄ and g-C₃N₄ are excited and the photoinduced holes and electrons are in their respective valence band (VB) and conduction band (CB). The energy band positions of valence band (VB) and conduction band (CB) can be calculated by the following equations:

$$E_{CB} = \chi - E_e - \frac{1}{2} E_g$$

$$E_{VB} = E_{CB} + E_g$$

Where χ is the absolute electronegativity of the semiconductor, E_e is the energy of free electrons on the hydrogen scale (4.5 eV) and E_g is the band gap of the semiconductor.⁶⁴ According to this equation and DRS analysis, the CB and VB potentials of g-C₃N₄ can be calculated to be -1.13 eV and 1.57 eV. Similarly, the CB and VB potentials of the compound Ni-CuWO₄ are found to be 0.51 eV and 2.41 eV respectively. It is seen from the Figure 11b

that the CB and VB of Ni-CuWO₄ is lower than that of g-C₃N₄. Again the energy difference between the CB of Ni-CuWO₄ and the VB of g-C₃N₄ is not too much. So, upon excitation, the photoinduced electrons transferred from the CB of Ni-CuWO₄ to the VB of g-C₃N₄ following a Z-scheme pathway thereby improving the separation process for photoinduced electron-hole pairs. The photogenerated electrons on the CB of g-C₃N₄ can cause decomposition of H₂O₂ under sunlight irradiation and produce OH⁻ and ·OH radical. Besides this, the electrons stored in the CB of g-C₃N₄ are captured by dissolved O₂ molecules and produce O₂⁻ radicals which again react with H⁺ from surface water to form H₂O₂ and subsequently produce ·OH radicals.⁶⁵ Furthermore, the photoinduced holes in the VB of Ni-CuWO₄ also react with adsorbed water molecules to generate ·OH radicals. The generated ·OH radicals further attack the benzene molecules and thereby produce hydroxylated benzene species in radical form. Upon further attacked by a ·OH radical, the hydroxylated benzene radical is converted to our desired product phenol with H₂O as only by-product. There is supposed to be another minor route where surface holes react with benzene molecule to form the corresponding intermediate which upon further reaction with dissolved oxygen molecule produces our required product phenol.⁶⁵

3.3.7 Structure Activity Correlation:

The geometry optimization, the g-C₃N₄ surface showed distortion due to the interaction of the g-C₃N₄ surface with the CuWO₄ (010) surface (Figure 12). The equilibrium distance between the g-C₃N₄ surface and the top of the CuWO₄ (010) surface is 2.215 Å. The calculated equilibrium adhesion energy per formula unit of CuWO₄ is -0.801 eV obtained from equation 1. The negative value of the adhesion energy suggests that the interaction of the g-C₃N₄ surface with CuWO₄ (010) surface is stabilizing.

$$E_{\text{ad}} = E_{\text{comp}} - E_{\text{g-C}_3\text{N}_4} - E_{\text{CuWO}_4(010)} \quad (1)$$

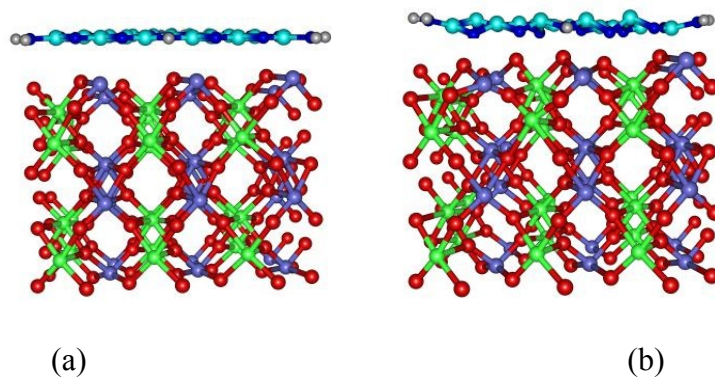


Figure 12. Model for simulating the interface between g-C₃N₄-CuWO₄ heterojunction, for geometry optimization (a) before optimization (b) after optimization.

To have a better understanding of the interaction of the g-C₃N₄ with CuWO₄ surface, it is important to study the interface electronic structure. Figure 13 shows the projected density of states (PDOS) of pure g-C₃N₄ surface, g-C₃N₄-CuWO₄ heterojunction surface and Ni doped g-C₃N₄-CuWO₄ heterojunction surface. The valence band maximum (VBM) of pure g-C₃N₄ is mainly composed of N 2p states while the conduction band maximum (CBM) has contribution from C 2p and N 2p hybridized state. In case of g-C₃N₄-CuWO₄ heterojunction, the VBM is composed of N 2p and O 2p hybridized state while the CBM is mainly composed of W 5d state. The involvement of W 5d state in the CBM of g-C₃N₄-CuWO₄ heterojunction may be the electronic factor towards the stability of the heterojunction. Moreover, there is a decrease in the band gap in the g-C₃N₄-CuWO₄ heterojunction compared to the pure g-C₃N₄ surface. The decrease in the band gap is more in the Ni-doped heterojunction (Figure 13c) which is expected to increase the optical activity of the heterojunction. This decrease in band gap may play a key role in optical excitation.

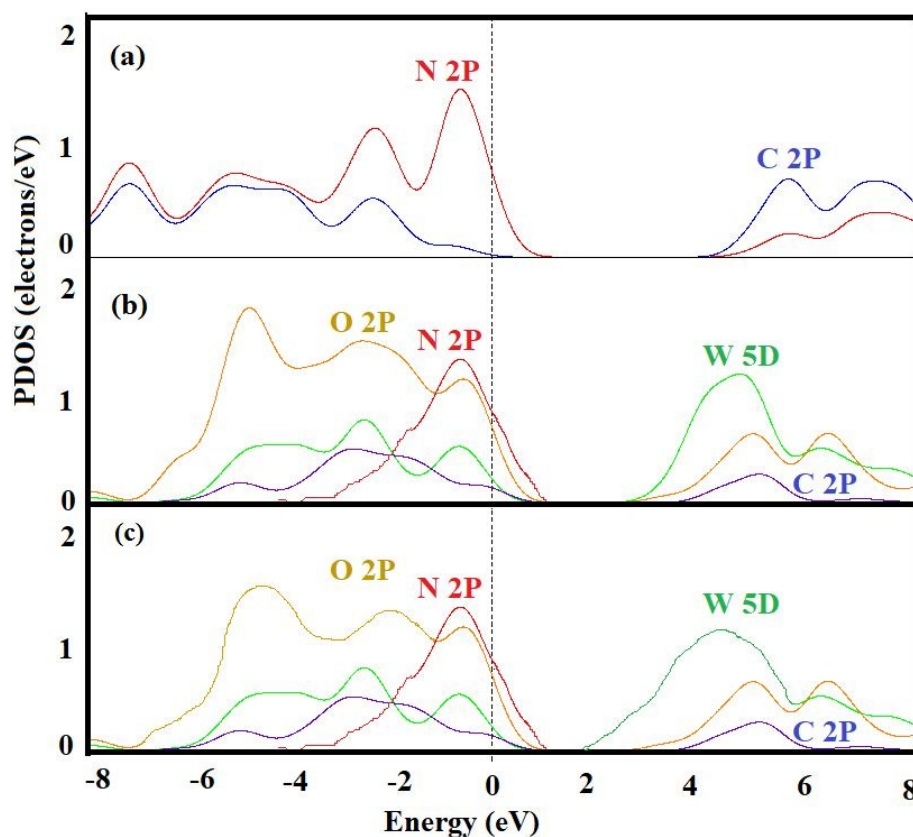


Figure 13. Projected density of states (PDOS) of (a) pure g-C₃N₄ surface, (b) g-C₃N₄-CuWO₄ heterojunction surface and (c) g-C₃N₄-Ni-CuWO₄ heterojunction surface. The dotted line represents the Fermi level.

We have also calculated the highest occupied surface crystal orbital (HOSCO), HOSCO-1, HOSCO-2 and the lowest unoccupied surface crystal orbital (LUSCO, LUSCO+1 and LUSCO+2) at the Γ -point to further understand the origin of visible light absorption. Figure 14 shows the respective orbitals. The HOSCO is mainly composed of N 2p orbital, in agreement with the PDOS analysis. The HOSCO-1 has contribution from N 2p and O 2p orbitals. The contribution of electron density of g-C₃N₄ vanishes at HOSCO-2. The LUSCO is composed mainly of W 5d orbitals. The normal photoexcitation of CuWO₄ takes place from O 2p orbital (HOSCO) to W 5d states. However, upon the composite formation with g-C₃N₄, some low energy gap bands forms which may enhance electron-hole pair separation leading to higher photocatalytic activity of the heterojunction. This was also confirmed from the optical studies like UV-DRS analysis, Tauc plot and PL spectroscopic analysis. Thus, our theoretical calculations provided a rationale at the microscopic level towards understand the mechanism of charge transfer and higher photocatalytic ability of the prepared composites.

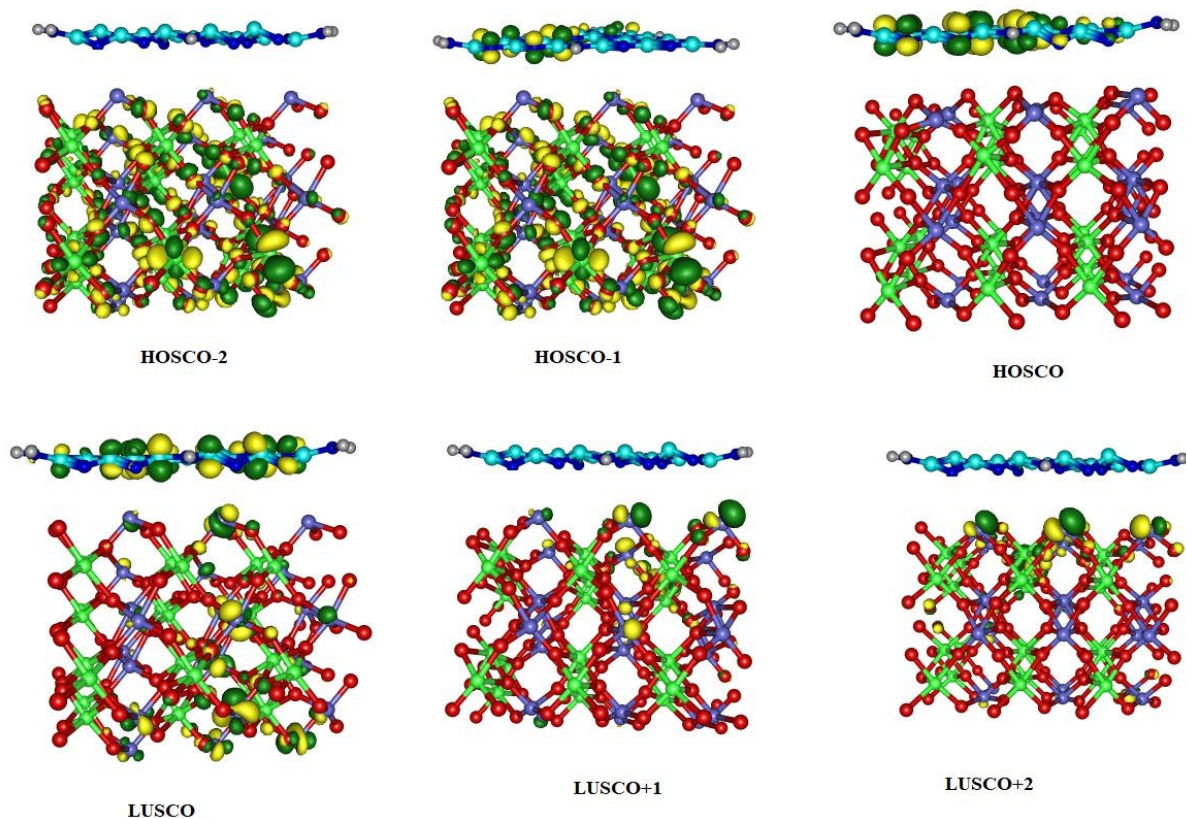


Figure 14. Γ -point orbital-isoamplitude surface of the respective orbitals.

3.3.7 Comparative study:

View Article Online
DOI: 10.1039/D0TA03729J

A comparative study of the optimised catalyst 0.2 Ni-CuWO₄/g-C₃N₄ was surveyed with other previously reported catalysts for the photocatalytic hydroxylation of benzene to phenol which is shown in the Table 4.

Table 4. Comparative study of different reported catalysts with our catalyst

Catalyst	Benzene conversion	Phenol yield	Reaction conditions	References
Cu ^{II} -based MOF	27.9%	27.1%	Catalyst-10 mg, benzene-1 mmol, H ₂ O, H ₂ O ₂ (30%)-1.25 mmol, 60°Celsius, 6 h, 40 W LED bulb	5
Ferrocene modified carbon nitride	Not known	14.4%	Catalyst-50 mg, benzene-0.8 mL (9 mmol), H ₂ O-4 mL, CH ₃ CN-4 mL, H ₂ O ₂ (30%)-0.51 mL (5 mmol), 4 h, 300 W xenon lamp	6
Au-Pd/g-C ₃ N ₄	24%	23.52%	Catalyst-10 mg, CH ₃ CN-5 mL, H ₂ O ₂ (25%)-2 mL, 2h, 100 W mercury lamp	22
Au@g-C ₃ N ₄	6%	3.42%	Catalyst-10 mg, CH ₃ CN-5 mL, H ₂ O ₂ (25%)-2 mL, 2h, 100 W mercury lamp	22
Fe-g-C ₃ N ₄	4.8%	0.39%	Catalyst-50 mg, benzene-0.8 mL (9 mmol), H ₂ O-4 mL, CH ₃ CN-4 mL, H ₂ O ₂ (30%)-0.51 mL (5 mmol), 4 h, 500 W xenon lamp	31
Fe-g-C ₃ N ₄ /SBA-15	11.9%	2.46%	Catalyst-50 mg, benzene-0.8 mL (9 mmol), H ₂ O-4 mL, CH ₃ CN-4 mL, H ₂ O ₂ (30%)-0.51 mL (5 mmol), 4 h, 500 W xenon lamp	31
BCW-4	5.8%	5.75%	Catalyst-50 mg, benzene-0.5 mmol), H ₂ O- 0.1 mL, CH ₃ CN-3 mL, O ₂ -3 mLmin ⁻¹ , 3 h, 300 W xenon lamp	65

Cu ₂ O-8/dG	30.18%	19.30%	Catalyst-5 mg, benzene-1 mmol, H ₂ O-5mL, CH ₃ CN-5mL, H ₂ O ₂ (30%)-1mmol, 16 h, white LED lamp (130 mWxcm ²)	66
Au/dG	30.06%	0.46%	Catalyst-5 mg, benzene-1 mmol, H ₂ O-5mL, CH ₃ CN-5mL, H ₂ O ₂ (30%)-1mmol, 16 h, white LED lamp (130 mWxcm ²)	66
CuAg@g-C ₃ N ₄	99%	Not known	Catalyst-25 mg, benzene-1 mmol, CH ₃ CH ₂ OH -5mL, CH ₃ CN-5mL, H ₂ O ₂ (30%)-1.1 mmol, 30 min, 20 W domestic bulb	67
g-C ₃ N ₄ /Cu/Pd	98.1%	87.8%	Catalyst-20 mg, benzene-0.5 mL, CH ₃ CN: H ₂ O-1:1, H ₂ O ₂ (30%)-5 mmol, 1.5 h, solar simulator	68
Ni-CuWO₄/g-C₃N₄ (0.2)	98.5%	81.5%	Catalyst-20 mg, benzene-1 mL (11.3 mmol), H₂O-0.2 mL, H₂O₂ (30%)-0.50 mL (4.5 mmol), 15 min, natural sunlight	This work

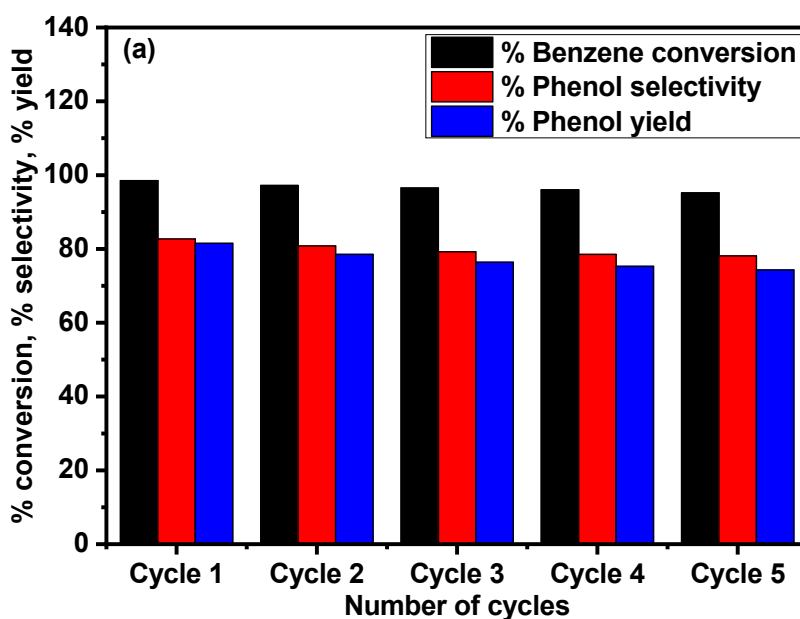
3.3.8 Catalyst recyclability:

Apart from the high catalytic activity, stability of the catalyst is also very important factor for the heterogeneous catalysis. To study the stability, recyclability of the 0.2 Ni-CuWO₄/g-C₃N₄ catalyst was performed. The reusability of the photocatalyst in the hydroxylation of benzene to phenol was evaluated under optimized reaction conditions (20 mg catalyst, 1 mL benzene, 0.2 mL H₂O, 0.5 mL H₂O₂) in presence of sunlight. Being heterogeneous in nature the catalyst could be easily separated from the reaction mixture after each run by centrifugation. The recovered catalyst was then directly used in the next catalytic run after washing and drying under the same reaction conditions. The results in Figure 15a demonstrates that the conversion of benzene decreases very slightly through five consecutive run resulting in 95.2% conversion of benzene with 78.1% selectivity and 74.3% yield of phenol in the fifth

run. As there is no massive change in the conversion of benzene in all the catalytic cycles, so it can be emphasized that the photocatalytic activity was almost kept stable during the recyclability experiment.

The recycled catalyst was also characterised by using techniques XPS and TEM analysis and details were included in the supporting information (Figure S2 and S3). The XPS analysis shows that there is no significant change of the signal peak positions. From TEM analysis, morphology is also found to be the same with that of the fresh catalyst.

To confirm the heterogeneous catalytic nature of the catalyst during the reaction, a filtration reaction is conducted. In this case after 10 minutes of the reaction, the solid catalyst was removed from the reaction mixture by centrifuge, and the reaction solution was subsequently allowed to react for another 50 minutes under the same reaction conditions. As shown in the Figure 15b, no further conversion of benzene is observed in the absence of catalyst. Therefore it can be demonstrated that there is no leaching of metal during the reaction which confirms the heterogeneous nature of the catalyst.



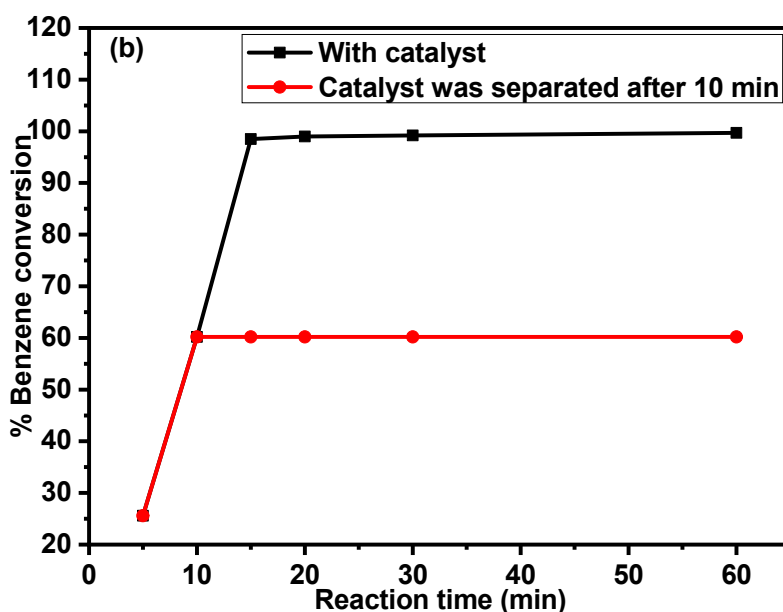


Figure 15. (a) Recyclability of 0.2 Ni-CuWO₄/g-C₃N₄ in the photocatalytic hydroxylation of benzene to phenol, (b) leaching experiment. Reaction conditions: catalyst (20 mg), benzene (1 mL, 11.3 mmol), H₂O (0.2 mL), H₂O₂ (0.5 mL), reaction time (15 min), sunlight.

4. Conclusion:

In conclusion, an inexpensive and environmental benign nanocomposite of Ni²⁺ substituted CuWO₄ crystal on graphitic carbon nitride was successfully synthesized to inhibit the rapid recombination of photoinduced holes and electrons. The well characterized catalysts by different physico-chemical, spectroscopic and microscopic techniques are found to be highly efficient for the photocatalytic hydroxylation of benzene to phenol under natural sunlight using H₂O₂ as an oxidant in presence of water. High benzene conversion of 98.5% with 82.7% selectivity and 81.5% yield of phenol were obtained only for 15 minutes of reaction in aqueous medium which was very efficient. The photocatalyst was also allowed to be reused under the optimized reaction conditions without significant diminution in photocatalytic activity. The theoretical study on highest occupied surface crystal orbital and the lowest unoccupied surface crystal orbital at the Γ -point to further understand the origin of visible light absorption and this study supports the experimental results on photocatalytic hydroxylation of benzene to produce phenol. Thus, the research thus emphasizes that a cost effective and efficient novel g-C₃N₄ supported Ni-CuWO₄ photocatalyst can be easily synthesized and this catalyst implies a new outlook for green and potential application towards photocatalysis for energy efficient process.

Associated content

View Article Online
DOI: 10.1039/D0TA03729J

Supporting Information

XRD spectra of the composites Ni-CuWO₄/g-C₃N₄ having different mass ratio, XPS data and TEM images of the recovered catalyst 0.2 Ni-CuWO₄/g-C₃N₄; percentage composition of main metal elements Cu, Ni and W of the as synthesised catalysts having different mass ratio, ¹H NMR and ¹³C NMR spectra of the products, GC graph of the products.

Author information

Corresponding Author

*E-mail: l.saikia@gmail.com/l.saikia@neist.res.in

Acknowledgements

The authors are thankful to the Director of CSIR-NEIST for allowing to publish the work. PB, LK acknowledges DST, New Delhi for providing the INSPIRE Fellowship, SB and LS are thankful to SERB-DST (Project No. GPP-0321) and DBT, New Delhi for financial support (Project No. GPP-0338) and PC and KS acknowledge CSIR and UGC JRF fellowship respectively.

References:

1. V. J. Liebig, *Ann. Pharm.*, 1834, **10**, 10.
2. A. S. Khayyat, R. Selvin and S. L. Roselin, *Applied Photosynthesis- New progress.*, 2016, **Chapter 8**, 147.
3. X. Lang, X. Chen and J. Zhao, *Chem. Soc. Rev.*, 2014, **43**, 473
4. D. Friedmann, A. Hakki, H. Kim, W. Choi and D. Bahnemann, *Green Chem.*, 2016, **18**, 5391.
5. L. Zhang, S. Qiu, G. Jiang, G. Jiang and R. Tang, *Asian J. Org. Chem.*, 2018, **7**, 165.
6. X. Ye, Y. Cui and X. Wang, *ChemSusChem*, 2014, **7**, 738.
7. Y. Zheng, B. Chen, P. Ye, K. Feng, W. Wang, Q.-Y. Meng, L.-Z. Wu and C.-H. Tung, *J. Am. Chem. Soc.*, 2016, **138**, 10080–10083.

8. G. Centi and S. Perathoner, *Catal. Today*, 2009, **143**, 145.
9. R. Molinari and T. Poerio, *Asia-Pac. J. Chem. Eng.*, 2010, **5**, 191.
10. J. R. Schmidt, *Appl. Catal. A: Gen.*, 2005, **280**, 89.
11. W. J. Han, J. Jung, M. Y. Lee and W. Nam, *Chem. Sci.*, 2017, **8**, 7119.
12. T. Yamada, A. Sakakura, S. Sakaguchi, Y. Obora and Y. Ishii, *New J. Chem.*, 2008, **32**, 738.
13. M. Tani, T. Sakamoto, S. Mita, S. Sakaguchi and Y. Ishii, *Angew. Chem. Int. Ed.*, 2005, **44**, 2586.
14. L. Balducci, D. Bianchi, R. Bortolo, R. D'Aloisio, M. Ricci, R. Tassinari and R. Ungarelli, *Angew. Chem. Int. Ed.*, 2003, **42**, 4937.
15. S. Fukuzumi and K. Ohkubo, *Asian J. Org. Chem.*, 2015, **4**, 836.
16. X. Cai, Q. Wang, Y. Liu, J. Xie, Z. Long, Y. Zhou and J. Wang, *ACS Sustainable Chem. Eng.*, 2016, **4**, 4986-4996.
17. J. Chen, J. Li, Y. Zhang and S. Gao, *Res. Chem. Intermed.*, 2010, **36**, 959.
18. S. Santra, H. Stoll and G. Rauhut, *Phys. Chem. Chem. Phys.* 2010, **12**, 6345.
19. A. Okemoto, Y. Tsukano, A. Utsunomiya, K. Taniya, Y. Ichihashi and S. Nishiyama, *J. Mol. Catal. A: Chem.*, 2016, **411**, 372.
20. X. Chen and F. Wang, J. Xu, *Top. Catal.*, 2011, **54**, 1016.
21. T. Miyake, M. Hamada, H. Niwa, M. Nishizuka and M. Oguri, *J. Mol. Catal. A: Chem.*, 2002, **178**, 199.
22. M. S. Hosseini, M. Ghiaci, A.S. Kulinich, W. Wunderlich, H. Farrokhpour, S. Mohammad and S. Ali, *J. Phys. Chem. C* 2018, **122**, 27477.
23. N. Hoffmann, *Chem. Rev.*, 2018, **108**, 1052.
24. C. B. D. V. Dasireddy and B. Likozar, *J. Taiwan Inst. Chem. Eng.*, 2018, **82**, 331.

25. Y. Wang, Y. Di, M. Antonietti, H. Li, X. Chen and X. Wang, *Chem. Mater.* **2010**, *22*, 5119. View Article Online
DOI: 10.1039/T0TA03729J
26. B. Lee, H. Naito and T. Hibino, *Angew. Chem., Int. Ed.*, 2012, **51**, 440.
27. P. Zhang, Y. Gong, H. Li, Z. Chen and Y. Wang, *RSC Adv.*, 2013, **3**, 5121.
28. Z. Zheng, B. Huang, X. Qin, X. Zhang, Y. Dai and H. M. Whangbo, *J. Mater. Chem. A.*, 2011, **21**, 9079.
29. X. Ye, Y. Cui, X. Qiu and X. Wang, *Appl. Catal. B: Env.*, 2014, **152-153**, 383.
30. M. Schulz, C. Paulik and G. Knör, *J. Mol. Catal. A: Chem.*, 2011, **347**, 60.
31. X. Chen, J. Zhang, X. Fu, M. Antonietti, X. Wang, *J. Am. Chem. Soc.* 2009, **131**, 11658.
32. J. Wang, A. S. Kondrat, Y. Wang, L. G. Brett, C. Giles, K. J. Bartley, L. Lu, Q. Liu, J. C. Kiely and J. G. J. Hutchings, *ACS Catal.*, 2015, **5**, 3575.
33. T. Zhang, D. Zhang, X. Han, T. Dong, X. Guo, C. Song, R. Si, W. Liu, Y. Liu and Z. Zhao, *J. Am. Soc.*, 2018, **140**, 16936-16940.
34. X. Xiong, H. Chen and Y. Xu, *J. Phys. Chem. C*, 2015, **119**, 5946.
35. A. Habibi-Yangjeh and M. Mousavi, *Adv. Powder Technol.*, 2018, **29**, 1379.
36. M. S. AlShehri, J. Ahmed, M. A. Alzahrani and T. Ahmed, *New J. Chem.*, 2017, **41**, 8178.
37. M. M. Mohamed, A. S. Ahmed and S. K. Khairou, *Appl. Catal. B: Env.*, 2014, **150-151**, 63.
38. K. Aneesh, R. S. S. Vusa and S. Berchmans, *Sens. and Actuators B: Chem.*, 2017, **253**, 723.
39. E. J. Yourey, B. J. Kurtz and M. B. Barlett, *J. Phys. Chem. C*. 2012, **116**, 3200.
40. Y. Zheng, J. Liu, J. Liang, M. Jaroniec and Z. S. Qiao, *Energy Environ. Sci.*, 2012, **5**, 6717.

41. F. Zhang, L. Huang, P. Ding, C. Wang, Q. Wang, H. Wang, Y. Li, H. Xu and H. Li, *J. Alloys Compd.*, 2019, **795**, 426. View Article Online
DOI: 10.1039/C9TA03729J
42. J. P. Perdew, K. Burke and M. Ernzerhof, *Phys. Rev. Lett.*, 1996, **77**, 3865.
43. M. Dolg, U. Wedig, H. Stoll and H. Preuss, *J. Chem. Phys.*, 1987, **86**, 866.
44. M. J. Frisch et. al. Gaussian 16, Revision A.03, Gaussian, Inc., Wallingford CT, 2016.
45. L. Tian, Multiwfn: A Multifunctional Wavefunction Analyzer (version 3.1). Available from: <http://Multiwfn.codeplex.com>. Accessed May 22, 2015.
46. J. M. Bojdys, O. Muller, M. Antonietti and A. Thomas, *Chem. Eur. J.*, 2008, **14**, 8177.
47. K. S. Pilli, G. T. Deutsch, E. T. Furtak, D. L. Brown, A. J. Turner and M. A. Herring, *Phys. Chem. Chem. Phys.*, 2013, **15**, 3273.
48. L. Zhu, J. Li, Q. Li, X. Liu, J. Meng and X. Cao, *Nanotechnology*, 2007, **18**, 055604.
49. J. Liu, T. Zhang, Z. Wang, G. Dawson and W. Chen, *J. Mater. Chem.*, 2011, **21**, 14398.
50. J. S. Naik and V. A. Salker, *Solid State Sci.*, 2010, **12**, 2065.
51. A. Raougi, F. Portemer, A. Quede and M. Marssi, *Appl. Surf. Sci.*, 1993, **153**, 1.
52. A. A. Said, M. M. M. Abd El-Wahab and M. Abd El-Aal, *Monatsh Chem.*, 2016, **147**, 1507.
53. H. He, J. Cao, M. Guo, H. Lin, J. Zhang, Y. Chen and S. Chen, *Appl. Catal. B: Env.*, 2019, **249**, 246.
54. D. Errandonea and J. Ruiz-Fuertes, *Crystal*, 2018, **8**, 71.
55. C. Ye, X. J. Li, J. Z. Li, B. X. Li, B. X. Fan, P. L. Zhang, B. Chen, H. C. Tung and Z. L. Wu, *ACS Catal.*, 2015, **5**, 6973.
56. J. Guzman, S. Carrettin and A. Corma, *J. Am. Chem. Soc.*, 2005, **127**, 3286.
57. J. Mao, Y. T. Peng, H. X. Zhang, K. Li, Q. L. Ye and L. Zan, *Catal. Sci. Technol.*, 2013, **3**, 1253.

58. D. Yang, T. Jiang, T. Wu, P. Zhang, H. Han, B. Han, *Catal. Sci. Technol.* 2016, **6**, 193. View Article Online
DOI: 10.1039/C5TA03729J
59. R. Gupta, B. Boruah, M. J. Modak and G. Madras, *J. Photochem. Photobiol. A* 2019, **372**, 108.
60. Y. Gao, O. Zandi and W. T. Hamann, *J. Mater. Chem. A*, 2016, **4**, 2826.
61. G. Chen, H. Guan, C. Dong, X. Xiao and Y. Wang, *J. Phys. Chem. Solids*, 2016, **98**, 209.
62. J. M. M. Sadiq and K. D. Bhat, *Ind. Eng. Chem. Res.*, 2016, **55**, 7267.
63. L. Ge, *Mater. Lett.*, 2011, **65**, 2652.
64. Z. Yu, Y. Su, Y. Yu, H. Wang, T. Qin, F. Zhang, Q. Shen and H. Yang, *Appl. Catal. B. Env.*, 2017, **213**, 127.
65. P. Chen, L. Chen, Y. Zeng, F. Ding, X. Jiang, N. Liu, C. T. Au and F. S. Yin, *Appl. Catal. B: Env.* 2018, **234**, 311.
66. J. He, M. Zhang, A. Primo, H. García and Z. Li, *J. Mater. Chem. A*, 2018, **6**, 19782.
67. S. Verma, N. B. R. Baig, N. M. Nadagouda and R. S. Varma, *ACS Sustain Chem. Eng.*, 2017, **5**, 3637.
68. Y. Zhang and S.-J. Park, *J. Catal.* 2019, **379**, 154.

Captions of Figures and Tables

Scheme 1. Reaction pathway for photocatalytic hydroxylation of benzene to phenol

Table 1. BET surface area analysis of the synthesized catalysts

Table 2. Photocatalytic hydroxylation of benzene to phenol over various catalysts

Table 3. Effect of light in photocatalytic hydroxylation of benzene to phenol over various catalysts

Table 4. Comparative study of different reported catalysts with our catalyst

Figure 1. Synthesis of Ni-CuWO₄@g-C₃N₄

Figure 2. PXRD pattern of as synthesized catalysts

Figure 3. FTIR spectra of as synthesized catalysts

Figure 4. Nitrogen adsorption-desorption isotherms of the as prepared samples.

Figure 5. (a) UV-DRS spectra, (b) Tauc plot, (c) PL spectra and (d) life time spectra of as synthesised catalysts.

Figure 6. TGA curves of pure g-C₃N₄ and composite 0.2 Ni-CuWO₄@g-C₃N₄

Figure 7. (a) XPS survey, (b) C1s XPS spectra, (c) N1s XPS spectra, (d) O1s XPS spectra, (e) Cu2p XPS spectra, (f) Ni2p XPS spectra and (g) W4f XPS spectra of catalyst 15% Ni-CuWO₄@g-C₃N₄

Figure 8. (a), (b) FESEM images of g-C₃N₄ and Ni-CuWO₄ respectively, (c) EDX pattern of composite 0.2 NCWCN, (d) and (e) TEM images of g-C₃N₄ and the composite 0.2 NCWCN respectively, (f) and (g) HRTEM images of 0.2 NCWCN and 0.2 CWCN respectively, (h) STEM image of composite 0.2 Ni-CuWO₄@g-C₃N₄

Figure 9. (a) to (f) elemental mapping of composite 0.2 Ni-CuWO₄@g-C₃N₄

Figure 10a. Effect of catalyst amount in photocatalytic hydroxylation of benzene to phenol under sunlight irradiation. Reaction conditions: catalyst from 10 mg to 30 mg, benzene (1 mL, 11.3 mmol), H₂O (0.2 mL), H₂O₂ (0.5 mL), reaction time (15 min), sunlight

Figure 10b. Effect of catalyst amount in photocatalytic hydroxylation of benzene to phenol under sunlight irradiation. Reaction conditions: catalyst (20 mg), benzene (1 mL, 11.3 mmol), H₂O (0.2 mL), H₂O₂ (0.5 mL), reaction time from 5 to 60 minutes, sunlight

Figure 10c. Effect of peroxide amount in photocatalytic hydroxylation of benzene to phenol under sunlight irradiation. Reaction conditions: catalyst (20 mg), benzene (1 mL, 11.3 mmol), H₂O (0.2 mL), H₂O₂ from 0.1 mL to 1 mL, reaction time (15 min), sunlight

Figure 11a. Photocatalytic hydroxylation of benzene to phenol with or without scavengers.
^aReaction conditions: catalyst (20 mg), benzene (1 mL, 11.3 mmol), H₂O (0.2 mL), H₂O₂ (0.5 mL), reaction time (15 min), scavengers (20 mmol)

Figure 11b. Plausible mechanism of photocatalytic hydroxylation of benzene to phenol

Figure 12. Model for simulating the interface between g-C₃N₄-CuWO₄ heterojunction for geometry optimization (a) before optimization (b) after optimization

Figure 13. Projected density of states (PDOS) of (a) pure g-C₃N₄ surface and (b) g-C₃N₄-CuWO₄ heterojunction surface. The dotted line represents the Fermi level

Figure 14. Γ -point orbital-isoamplitude surface of the respective orbitals.

Figure 15. (a) Recyclability of 0.04 Ni-CuWO₄@g-C₃N₄ in the photocatalytic hydroxylation of benzene to phenol, (b) leaching experiment. Reaction conditions: catalyst (20 mg), benzene (1 mL, 11.3 mmol), H₂O (0.2 mL), H₂O₂ (0.5 mL), reaction time (15 min), sunlight.

Table of Contents

View Article Online
DOI: 10.1039/D0TA03729J

Efficient hydroxylation of benzene to phenol by H_2O_2 using Ni doped CuWO_4 on carbon nitride as catalyst under solar irradiation and its structure activity correlation

Purashri Basyach,^{ab} Ankur Kanti Guha^c, Sukanya Borthakur,^{ab} Lisamoni Kalita,^{ab} PubaliChetia,^{ab} Karanika Sonowal^{ab} and Lakshi Saikia^{*ab}

^a Materials Science & Technology Division, CSIR-North East Institute of Science and Technology, Jorhat-785006, Assam, India

^b Academy of Scientific and Innovative Research, New Delhi, India

^c Department of Chemistry, Cotton University, Panbazar, Guwahati-781001

